

Role of quantum fluctuations in a system with strong fields: Onset of hydrodynamical flow

Kevin Dusling⁽¹⁾, Thomas Epelbaum⁽²⁾,
François Gelis⁽²⁾, Raju Venugopalan⁽¹⁾

October 22, 2018

1. Physics Department
Brookhaven National Laboratory
Upton, NY-11973, USA
2. Institut de Physique Théorique (URA 2306 du CNRS)
CEA/DSM/Saclay
91191, Gif-sur-Yvette Cedex, France

Abstract

Quantum fluctuations are believed to play an important role in the thermalization of classical fields in inflationary cosmology but their relevance for isotropization/thermalization of the classical fields produced in heavy ion collisions is not completely understood. We consider a scalar ϕ^4 toy model coupled to a strong external source, like in the Color Glass Condensate description of the early time dynamics of ultrarelativistic heavy ion collisions. The leading order classical evolution of the scalar fields is significantly modified by the rapid growth of time-dependent quantum fluctuations, necessitating an all order resummation of such “secular” terms. We show that the resummed expressions cause the system to evolve in accordance with ideal hydrodynamics. We comment briefly on the thermalization of our quantum system and the extension of our results to a gauge theory.

1 Introduction

A remarkable outcome of the heavy ion experiments at RHIC [1–4] is the large elliptic flow observed in the collisions. Phenomenological hydrodynamical models that fit the RHIC data appear to require that the quark gluon matter has a very small value for the dimensionless ratio of the viscosity to the entropy density [5]. This ratio η/s , a measure of the “perfect fluidity” of the system, is estimated to be $\lesssim 5/4\pi$ [6], where $\eta/s = 1/4\pi$ is a conjectured universal lower

bound [7,8]. It was shown recently [9–11] that the degree of perfectness of the quark-gluon fluid produced at RHIC is sensitive to details of the initial spatial distribution of the produced matter at the onset of hydrodynamic flow.

An important feature of the hydrodynamic models is that they require very early thermalization after the collision. Estimates for the thermalization time, which range from $\tau_{\text{relax}} \sim 0.6 - 1$ fm [12–14], are difficult to reconcile with a simple picture of thermalization arising from the rapid scattering of quasi-particles at rates greater than the expansion rate of the fluid. The uncertainty principle tells us that for $\tau_{\text{relax}} \leq 1$ fm, modes with momenta ~ 200 MeV are not even on-shell, let alone amenable to being described as quasi-particles undergoing scattering. While a quasi-particle description is not essential to thermalization, it is the simplest one, and other realizations are more complicated. With regard to the issue of flow however, it is sufficient to note that one requires primarily that matter be isotropic and (nearly) conformal to obtain a closed form expression for the hydrodynamic equations [15].

How isotropization and (subsequently) thermalization is achieved in heavy ion collisions is an outstanding problem which requires that the problem be considered *ab initio*. What this means is that one needs to understand and compute the properties of the relevant degrees of freedom in the nuclear wavefunctions and how these degrees of freedom decohere in a collision to produce quark-gluon matter. An *ab initio* approach to the problem can be formulated within the framework of the Color Glass Condensate (CGC) effective field theory, which describes the relevant degrees of freedom in the nuclei as dynamical classical fields coupled to static color sources [16–18]. The computational power of this approach is a consequence of the dynamical generation of a semi-hard scale, the saturation scale [19,20], which allows a weak coupling treatment of the relevant degrees of freedom [21–23] in the high energy nuclear wavefunctions.

There has been significant progress recently in applying the CGC effective field theory to studying the early time behavior of the matter produced in heavy ion collisions. Inclusive quantities such as the pressure and the energy density in this matter (called the Glasma [24]) can be written as expressions that factorize the universal properties of the nuclear wavefunctions (measurable for instance in proton-nucleus or electron-nucleus collisions) from the detailed dynamics of the matter in collision [25–27]. Key to this approach are the quantum fluctuations around the classical fields in the wavefunctions and in the collision. Quantum fluctuations that are invariant under boosts can be isolated in universal functions that evolve with energy. There are however also quantum fluctuations that are not boost invariant which are generated during the collision. These quantum fluctuations can grow rapidly and therefore play a significant role in the subsequent temporal evolution of the Glasma.

The problem of how to treat these so-called “secular divergences” of perturbative series is very general and occurs in a wide variety of dynamical systems [28]. In particular, the role of time dependent quantum fluctuations in heavy ion collisions bears a strong analogy to their role in the evolution of the early universe [29]. In the latter case, quantum fluctuations around a rapidly decaying classical field, the inflaton, are enhanced due to parametric resonance,

and it is conjectured that this dynamics termed “preheating” [30] may lead to turbulent thermalization [31] in the early universe.

It is therefore very important to understand the precise role of these quantum fluctuations in heavy ion collisions to determine whether they play an analogous role to that in the early universe in the isotropization/thermalization of the system. Their computation in a gauge theory is quite involved so for simplicity, we shall in this paper first attack this problem in a scalar ϕ^4 field theory. Like QCD, the coupling is dimensionless in this theory and the fields are self interacting. In addition, we choose initial conditions for our study that are similar to those in the CGC treatment of heavy ion collisions. It must be said at the outset that there are important differences between the two theories and there is no *a priori* guarantee that the lessons learnt in one case will translate automatically to the other.

The CGC initial conditions, for weak couplings $g \ll 1$, specifically lead to a power counting scheme where the leading contribution to inclusive quantities is the classical contribution of order $\mathcal{O}(1/g^2)$. Quantum corrections begin at $\mathcal{O}(1)$ and their contribution can be expressed as real-time partial differential equations for small fluctuations in the classical background, with purely retarded initial conditions. We will show that there are modes of the small fluctuation field that grow very rapidly and can become as large as the classical field on time scales of interest in the problem. We observe that there are two sorts of rapidly growing modes of the fluctuation field. One are modes that enjoy parametric resonance and grow exponentially. These modes are however localized in a rather narrow resonance band. The zero mode and low lying modes grow linearly and can also influence the temporal evolution of the system. Both sorts of “secular” terms can be isolated and resummed to all orders in perturbation theory. The resulting expressions are stable and can be expressed as an ensemble average over a spectrum of quantum fluctuations convolved with the *leading order* inclusive quantity which, for a particular fluctuation field, is a functional of the classical field shifted by that quantum fluctuation. We note that a similar observation was made previously in the context of inflationary cosmology [32–34].

The fact that one can express resummed expressions for the pressure and energy density as ensemble averages over quantum fluctuations has profound consequences. Without resummation, the relation between the energy density and the pressure is not single valued. For the resummed expressions, while the relation between the pressure and energy density is not single valued at early times, it becomes so after a finite evolution time. This development of an “equation of state” therefore allows one to write the conservation equation for the resummed energy momentum tensor $T^{\mu\nu}$ as a closed form set of equations, which are the equations of ideal hydrodynamics. This of course suggests that the system behaves as a perfect fluid. If the considerations in our paper can be applied to a gauge theory, the result would have significant ramifications for the interpretation of the heavy ion experiments and the extraction of η/s in hydrodynamical models.

The evolution of the system towards the equation of state characteristic of hydrodynamic flow can be interpreted as arising from a phase decoherence of

the different classical trajectories of the energy momentum tensor for different initial conditions given by the ensemble of quantum fluctuations. For a scalar ϕ^4 theory, the frequency of the periodic classical trajectories is proportional to the amplitude. Therefore, for different initial values of the amplitude, the different trajectories are phase shifted. The ensuing cancellations between trajectories results in the single valued relation between the pressure and the energy density. While it appears that decoherence can arise from the zero mode and near lying modes alone, the inclusion of the resonant band significantly alters the decoherence of the system. Similar behavior has been seen in models of reheating after inflation [35–37]. In particular, one sees that quantum de-coherence of the inflaton field leads to a transition from a dust-like equation of state to a radiation dominated era.

It is interesting to ask whether the decoherence and concomitant fluidity observed in our numerical simulations implies thermalization of the system. We first investigate the behavior of the ensemble of initial conditions in the *Poincaré* phase plane for the toy case of uniform background field and fluctuations. One sees that the initially localized trajectories spread around a close loop filling the phase-space as one would expect for the phase-space density of a micro-canonical ensemble. For the toy example considered, the ensemble average of the trace of the energy momentum tensor can be expressed at large times as the time average along a single trajectory in the *Poincaré* phase plane. For the scale invariant ϕ^4 theory, this average is zero with the consequence that the energy momentum tensor becomes traceless resulting in a single valued relation between the energy density and the pressure.

Going beyond the toy example, for the general case of spatially non-uniform fluctuations, there is no easy way to visualize trajectories on the *Poincaré* phase plane because the system is infinite dimensional. However, because the numerical problem is formulated on a lattice, one can look at a small sub-system on this lattice and study its event-by-event energy fluctuations. Starting from a Gaussian initial distribution, we see that the distribution converges to an exponential form. One can also study the moments of the energy distribution; these again demonstrate a rapid change from initial transient values to stationary values. While the behavior is close to those expected from a canonical thermal ensemble, it is premature from our present studies to make definitive conclusions. This will require a careful study of the effects of varying the coupling and volume effects and will be left to a future study.

We note however that the formalism developed in our paper is well suited to the study of thermalization of quantum systems¹. It has been argued previously [38–41] that quantum systems will thermalize if they satisfy Berry’s conjecture [42]. This conjecture states that the high lying quantum eigenstates of a system whose classical behavior is chaotic and ergodic have a wavefunction that behaves as a linear superposition of plane waves whose coefficients are Gaussian random variables. When an inclusive measurement is performed

¹We thank Giorgio Torrieri for bringing to our attention Berry’s conjecture and the accompanying literature on eigenstate thermalization.

on such an eigenstate, one obtains results that agree with the predictions of the micro-canonical equilibrium ensemble, a property that has been dubbed “eigenstate thermalization” in [39]. If the state at $t = 0$ is a coherent superposition of such eigenstates, the micro-canonical predictions become valid only after the states in the superposition have sufficiently decohered—thus for quantum systems where Berry’s conjecture apply, thermalization appears to be a consequence of decoherence. The ensemble of quantum fluctuations included via the resummation we develop in the section 2.6 leads to fields that have precisely this behavior (see eqs. (51-52)). Our interest ultimately is in QCD, where the classical behavior of the system is believed to be chaotic [43–45]. Because much of our formalism can be extended to gauge theories, we anticipate that a first principles treatment of thermalization is feasible.

This paper is organized as follows. In section 2, we introduce the model scalar theory and the CGC-like initial conditions for its temporal evolution. We then discuss the computation of $T^{\mu\nu}$ at leading and next-to-leading order. The problem of secular divergences is noted, and a stable resummation procedure is developed. A simplified toy model is considered in section 3, wherein only spatially uniform fluctuations are considered. The behavior of the resummed pressure and energy density and their relaxation to an equation of state is studied. These results are interpreted and understood as a consequence of the decoherence of the system which allows one to equate ensemble averages to a temporal average over individual classical trajectories. For the longitudinally expanding case, temporal evolution in the toy model displays the behavior of a fluid undergoing ideal hydrodynamic flow. The full quantum field theory is considered in section 4, where we compute *ab initio* the spectrum of fluctuations. The full theory displays the same essential features as the toy model studied in section 3, albeit the interplay of linearly growing low lying momentum modes and the resonant modes leads to a more complex temporal evolution. In this section, we also investigate the dependence of the relaxation time on the strength of the coupling constant. Then, we study the energy distribution in a small subsystem, and its time evolution. We conclude with a brief outlook. Much of the details of the computation are given in appendices. In appendix A, we discuss the numerical solution of the scalar field model, including the lattice discretization, the computation of the quantum fluctuation spectrum and the sensitivity of the results to the ultraviolet cut-off. The stability analysis of linearized perturbations to the classical field is considered in Appendix B. The resonance band is identified and the Lyapunov exponents are computed explicitly. We also discuss the relationship between decoherence and linear instabilities.

2 Temporal evolution of $T^{\mu\nu}$

In this section, we will consider a scalar field toy model whose behavior mimics key features of the Glasma [24] description of the early behavior of the quark-gluon matter produced in high energy heavy ion collisions. In the CGC framework, strong color fields are present in the initial conditions for the evolution of

the Glasma. In this situation, the leading order contribution is given by classical fields, with higher order corrections coming from the *apparently* sub-leading quantum fluctuations. We consider the stress-energy tensor in this scalar field model and discuss its temporal evolution at leading (LO) and next-to-leading orders (NLO). We show explicitly that there are contributions at NLO that can grow with time and become larger than the LO terms. We end this section by describing how these “secular” terms can be resummed and the results expressed in terms of an average over a Gaussian ensemble of classical fields.

2.1 Scalar model with CGC-like initial conditions

Our CGC inspired scalar model has the Lagrangean

$$\mathcal{L} \equiv \frac{1}{2}(\partial_\mu \phi)(\partial^\mu \phi) - \frac{g^2}{4!}\phi^4 + J\phi, \quad (1)$$

where J is an external source. In the CGC framework, the source J coupled to the gauge fields represents the color charge current carried by the two colliding heavy ions. The current is zero at positive proper time, corresponding to times after the collision has taken place. We emulate this feature of the CGC in a simpler coordinate system by taking the source J to be nonzero only for Cartesian time $x^0 < 0$, and parameterize it as²

$$J(x) \sim \theta(-x^0) \frac{Q^3}{g}. \quad (2)$$

At $x^0 > 0$, where J is zero, the fields evolve solely via their self-interactions, in an analogous fashion to the non-Abelian color fields produced in the collision of two hadrons or nuclei.

In eq. (2), we incorporated two additional features of the CGC. The first feature corresponds to a strong external current J , which follows from the power of the inverse coupling when $g \ll 1$; weak coupling is essential to motivate an expansion in powers of g^2 . The other feature of the CGC that is emulated is that the dimensionful parameter Q in eq. (2) plays a role analogous to that of the saturation scale [19,20], in the sense that non-linear interactions are sizeable for modes $|\mathbf{k}| \lesssim Q$.

Note that a scalar field theory with a ϕ^4 coupling in four space-time dimensions is scale invariant at the classical level—the coupling constant g is dimensionless in the theory. In our model, this scale invariance is broken by the coupling of the scalar field to the external source J containing the dimensionful scale Q . We may therefore anticipate that all physical quantities are simply expressed by the appropriate power of Q times a prefactor that depends on g .

²In the numerical implementation of the model, the time dependent prefactor is constrained to vanish when $x^0 \rightarrow -\infty$ to ensure a free theory in the remote past.

2.2 $T^{\mu\nu}$ at leading order

Because the source J contains a power of the inverse coupling, the power counting for Feynman diagrams indicates that the order of magnitude of a given graph depends only on its number of external lines and number of loops, but not on the number of sources J attached to the graph [46,47]. For the energy-momentum tensor of the theory, the various contributions can be organized in a series in powers of g^2 as

$$T^{\mu\nu} = \frac{Q^4}{g^2} \left[c_0 + c_1 g^2 + c_2 g^4 + \dots \right]. \quad (3)$$

In this expansion, the coefficients c_0, c_1, c_2, \dots are themselves infinite series in the combination gJ corresponding to an infinite set of Feynman diagrams. This combination is parametrically independent of g because $J \sim g^{-1}$. More precisely, c_0 contains only tree diagrams, c_1 1-loop diagrams, c_2 2-loop diagrams, and so on.

In our model, the leading order (tree level) contribution to the energy-momentum tensor can be expressed solely in terms of a classical solution φ of the field equation of motion [46]. Namely, one has

$$T_{\text{LO}}^{\mu\nu}(x) = c_0 \frac{Q^4}{g^2} = \partial^\mu \varphi \partial^\nu \varphi - g^{\mu\nu} \left[\frac{1}{2} (\partial_\alpha \varphi)^2 - \frac{g^2}{4!} \varphi^4 \right], \quad (4)$$

where

$$\begin{aligned} \square \varphi + \frac{g^2}{3!} \varphi^3 &= J, \\ \lim_{x^0 \rightarrow -\infty} \varphi(x^0, \mathbf{x}) &= 0. \end{aligned} \quad (5)$$

Clearly, due to the non-linear term in the equation of motion, the solution φ (and hence the coefficient c_0) depends on gJ to all orders, as stated previously. This LO energy momentum tensor is conserved³,

$$\partial_\mu T_{\text{LO}}^{\mu\nu} = 0. \quad (6)$$

If the source J is taken to be spatially homogeneous, then the energy-momentum tensor evaluated at leading order has the simple form

$$T_{\text{LO}}^{\mu\nu}(x) = \begin{pmatrix} \epsilon_{\text{LO}} & 0 & 0 & 0 \\ 0 & p_{\text{LO}} & 0 & 0 \\ 0 & 0 & p_{\text{LO}} & 0 \\ 0 & 0 & 0 & p_{\text{LO}} \end{pmatrix}, \quad (7)$$

with the leading order energy density and pressure given by

$$\begin{aligned} \epsilon_{\text{LO}} &= \frac{1}{2} \dot{\varphi}^2 + \frac{g^2}{4!} \varphi^4 \\ p_{\text{LO}} &= \frac{1}{2} \dot{\varphi}^2 - \frac{g^2}{4!} \varphi^4. \end{aligned} \quad (8)$$

³Strictly speaking, this is true only at $x^0 > 0$. At negative times, some energy is injected into the system by the external source J .

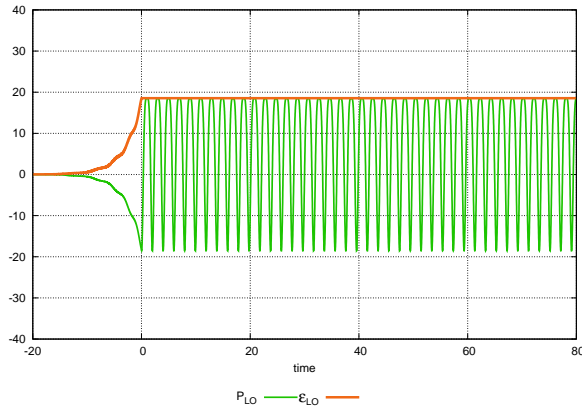


Figure 1: Components of $T_{\text{LO}}^{\mu\nu}$ for a spatially uniform external source. To perform this calculation, we took in eq. (5) a source $J = g^{-1}Q^3\theta(-x^0)e^{bQx^0}$ (with $g = 1, b = 0.1$ and $Q = 2.5$), that vanishes adiabatically in the remote past.

One can easily check that the energy density ϵ_{LO} is constant in time at $x^0 > 0$ (after the external source J has been switched off), while the pressure p_{LO} is a periodic function of time at $x^0 > 0$, as illustrated in the figure 1. From the numerical computation, it is clear that at this order of the calculation of ϵ_{LO} and p_{LO} , one does not have a well defined (single valued) relationship $\epsilon_{\text{LO}} = f(p_{\text{LO}})$. In other words, *there is no equation of state at leading order in g^2* . This might appear problematic at the outset because one might expect that the scale invariance of the theory would require the energy momentum tensor to be traceless. As discussed further in section 3.4.2, this is not so for the case of a scalar theory.

2.3 $T^{\mu\nu}$ at next to leading order

At next-to-leading order, the energy momentum tensor can be written as

$$\begin{aligned}
T_{\text{NLO}}^{\mu\nu} &= c_1 Q^4 = \partial^\mu \varphi \partial^\nu \beta + \partial^\mu \beta \partial^\nu \varphi - g^{\mu\nu} \left[\partial_\alpha \beta \partial^\alpha \varphi - \beta V'(\varphi) \right] + \\
&+ \int \frac{d^3 \mathbf{k}}{(2\pi)^3 2k} \left[\partial^\mu a_{-\mathbf{k}} \partial^\nu a_{+\mathbf{k}} - \frac{g^{\mu\nu}}{2} \left(\partial_\alpha a_{-\mathbf{k}} \partial^\alpha a_{+\mathbf{k}} - V''(\varphi) a_{-\mathbf{k}} a_{+\mathbf{k}} \right) \right],
\end{aligned} \tag{9}$$

where for brevity we use the notation $V(\varphi) \equiv g^2 \varphi^4 / 4!$ with each prime denoting a derivative with respect to φ . In this formula, β and $a_{\pm \mathbf{k}}$ are small field

perturbations, that are defined by the following equations:

$$\begin{aligned}
& \left[\square + V''(\varphi) \right] a_{\pm \mathbf{k}} = 0 \\
& \lim_{x^0 \rightarrow -\infty} a_{\pm \mathbf{k}}(x) = e^{\pm i \mathbf{k} \cdot x} , \\
& \left[\square + V''(\varphi) \right] \beta = -\frac{1}{2} V'''(\varphi) \int \frac{d^3 \mathbf{k}}{(2\pi)^3 2k} a_{-\mathbf{k}} a_{+\mathbf{k}} \\
& \lim_{x^0 \rightarrow -\infty} \beta(x) = 0 .
\end{aligned} \tag{10}$$

Because the classical field φ is spatially homogeneous in the toy model considered here, the equation of motion for $a_{\pm \mathbf{k}}$ simplifies to

$$\ddot{a}_{\pm \mathbf{k}} + (\mathbf{k}^2 + V''(\varphi)) a_{\pm \mathbf{k}} = 0 , \tag{11}$$

and the field fluctuation β depends only on time.

After some algebra, it is easy to check that the energy-momentum tensor is also conserved at NLO⁴ for $x^0 > 0$,

$$\partial_\mu T_{\text{NLO}}^{\mu\nu} = 0 . \tag{12}$$

The 00 component of $T_{\text{NLO}}^{\mu\nu}$ in eq. (9) gives us the energy density at NLO,

$$\epsilon_{\text{NLO}} = \dot{\beta} \dot{\varphi} + \beta V'(\varphi) + \frac{1}{2} \int \frac{d^3 \mathbf{k}}{(2\pi)^3 2k} \left[\dot{a}_{-\mathbf{k}} \dot{a}_{+\mathbf{k}} + (\mathbf{k}^2 + V''(\varphi)) a_{-\mathbf{k}} a_{+\mathbf{k}} \right] . \tag{13}$$

Given eqs. (10), it is straightforward to verify that this correction is also constant in time, $\dot{\epsilon}_{\text{NLO}} = 0$, in agreement with eq. (12). The 11 component of eq. (9) –the NLO pressure in the x direction– reads

$$p_{\text{NLO}} = \dot{\beta} \dot{\varphi} - \beta V'(\varphi) + \frac{1}{2} \int \frac{d^3 \mathbf{k}}{(2\pi)^3 2k} \left[\dot{a}_{-\mathbf{k}} \dot{a}_{+\mathbf{k}} - (\mathbf{k}^2 - 2k_x^2 + V''(\varphi)) a_{-\mathbf{k}} a_{+\mathbf{k}} \right] . \tag{14}$$

Note that although the integrand is not rotationally invariant, the result of the \mathbf{k} integration is symmetric and the NLO pressures are the same in all directions.

We evaluated numerically ϵ_{NLO} and p_{NLO} for a coupling constant $g = 1$, by first solving eqs. (10) for β and for the $a_{\mathbf{k}}$'s (for a discretized set of \mathbf{k} 's). The results of this calculation are shown in the figure 2. From this evaluation, we see that the energy density at NLO is constant at $x^0 > 0$, as we expected⁵. We also notice that for $g = 1$, the NLO correction to the energy density is very small, of the order of 1.4% of the LO result⁶. Thus, we conclude from

⁴This result should be self-evident because the conservation equation $\partial_\mu T^{\mu\nu} = 0$ is linear in the components of $T^{\mu\nu}$. Therefore, it does not mix the different g^2 orders, requiring the conservation equation to be satisfied for each order in g^2 .

⁵This time independence can be seen as a test of the accuracy of the numerical calculation, because it results from a cancellation between several terms that grow with time.

⁶Indeed, since there is a prefactor $1/4!$ in our definition of the interaction potential, $g = 1$ corresponds to fairly weak interactions.

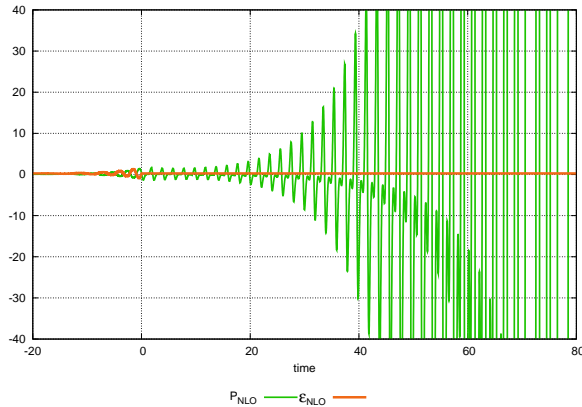


Figure 2: Components of $T_{\text{NLO}}^{\mu\nu}$ for a spatially uniform external source. This calculation was performed for $g = 1$.

this that for such a value of the coupling, we have a well behaved perturbative expansion for ϵ . The NLO pressure however behaves quite differently. Not only it is varying in time (hence no equation of state at NLO), but it also has oscillations whose amplitude grows exponentially at large x^0 . Therefore, the NLO correction to the pressure eventually becomes larger than the LO contribution, and the perturbative expansion for the pressure in powers of g^2 breaks down⁷. Also noteworthy is the fact that at $x^0 = 0$, p_{NLO} is still a small correction to p_{LO} ; it only becomes large at later times.

2.4 Interpretation of the NLO result

The secular divergence of the pressure at NLO can be understood as a consequence of the unstable behavior of $a_{\pm\mathbf{k}}(x)$ for some values of \mathbf{k} . The stability analysis of small quantum fluctuations in ϕ^4 field theory is performed in appendix B. From this study, one obtains the following results:

- i. There is a range in $|\mathbf{k}|$ where the $a_{\pm\mathbf{k}}$'s diverge exponentially in time, due to the phenomenon of parametric resonance.
- ii. The zero mode $\mathbf{k} = 0$ fluctuation, a_0 , diverges linearly in time, a phenomenon closely related to the fact that the oscillation frequency in a non-harmonic potential depends on the amplitude of the oscillations.

In addition, one observes numerically that fluctuation modes in the vicinity of $\mathbf{k} = 0$, albeit not mathematically unstable, can attain quite large values. (They appear to grow linearly for some time before decreasing in value.)

⁷A similar behavior was observed in a different context in [48].

Because of the existence of modes that grow in time, integrals such as

$$I(x^0) \equiv \int \frac{d^3 \mathbf{k}}{(2\pi)^3 2k} a_{-\mathbf{k}}(x) a_{+\mathbf{k}}(x), \quad (15)$$

that appear in the components of $T_{\text{NLO}}^{\mu\nu}$ (see eqs. (13) and (14)) or in the right hand side of the equation (eq. (10)) for β , are divergent when $x^0 \rightarrow +\infty$ as illustrated in the figure 3. In this plot, one can check that the envelope of the

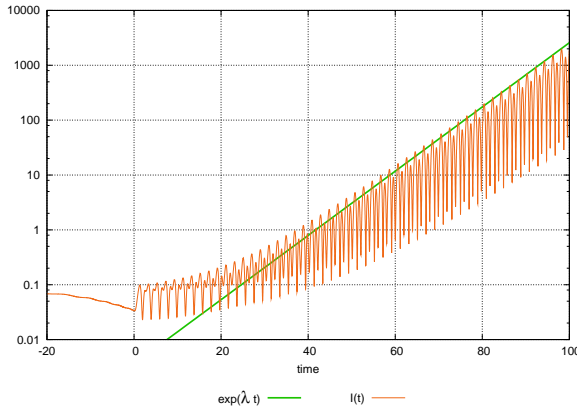


Figure 3: Numerical evaluation of the integral defined in eq. (15). The line denotes an exponential fit to the envelope.

oscillations grows exponentially, with a growth rate $\lambda \approx 2 * \mu_{\text{max}}$ where μ_{max} is the maximal Lyapunov exponent in the resonance band. If the integral in eq. (15) is evaluated with an upper cutoff that excludes the resonance band from the integration domain, then $I(x^0)$ grows only linearly, because now its behavior is dominated by the soft fluctuation modes whose growth is linear.

Even though secular divergences in integrals such as eq. (15) are present in eq. (13), they cancel in the calculation of ϵ_{NLO} because the energy density in our toy model is protected by the conservation of the energy momentum tensor. However, they do not cancel in p_{NLO} which explains the divergent behavior displayed in fig. 2.

2.5 Alternate form of $T^{\mu\nu}$ at NLO

The secular divergence of the pressure at NLO suggests that the weak coupling series for the pressure may be better behaved if one develops a resummation scheme that captures the physics of the secular terms by identifying their contribution and summing them to all orders in perturbation theory. Before we do this, we shall discuss a general formulation of the energy-momentum tensor at NLO which will help formulate the problem of resumming secular terms.

In previous works [46,47], we showed that the problem of computing NLO corrections for *inclusive* quantities—such as components of the energy momentum tensor in field theories with strong sources—could be formulated as an initial value problem. Specifically, for the energy-momentum tensor, we can write the NLO contribution at an arbitrary space-time point as the action of a functional operator acting on the LO contribution,

$$T_{\text{NLO}}^{\mu\nu}(x) = \left[\int d^3\mathbf{u} \beta \cdot \mathbb{T}_{\mathbf{u}} + \frac{1}{2} \int d^3\mathbf{u} d^3\mathbf{v} \int \frac{d^3\mathbf{k}}{(2\pi)^3 2k} [a_{+\mathbf{k}} \cdot \mathbb{T}_{\mathbf{u}}][a_{-\mathbf{k}} \cdot \mathbb{T}_{\mathbf{v}}] \right] T_{\text{LO}}^{\mu\nu}(x), \quad (16)$$

The operator $\mathbb{T}_{\mathbf{u}}$ that appears in eq. (16) is the generator of shifts of the initial conditions $\varphi_0, \partial_0\varphi_0$ (at $x^0 = 0$) of the classical field,

$$a \cdot \mathbb{T}_{\mathbf{u}} \equiv a(0, \mathbf{u}) \frac{\delta}{\delta\varphi_0(\mathbf{u})} + \dot{a}(0, \mathbf{u}) \frac{\delta}{\delta\partial_0\varphi_0(\mathbf{u})}. \quad (17)$$

The factor $T_{\text{LO}}^{\mu\nu}$ in the functional formulation of eq. (16) should therefore be considered as a functional of the value of $\varphi, \dot{\varphi}$ at $x^0 = 0$. The full content of the temporal NLO evolution of $T^{\mu\nu}$ is contained in eq. (16). One can check that this expression is exactly equivalent to eq. (9) [25].

The expression in eq. (16) has been obtained by splitting the time evolution at $x^0 = 0$ such that the $x^0 < 0$ part of the time evolution is described by the operator in the square brackets, and the evolution at $x^0 > 0$ is hidden in the functional dependence of $T_{\text{LO}}^{\mu\nu}$ with respect to the value of the classical field φ at $x^0 = 0$. The choice of $x^0 = 0$ for this split in the time evolution is arbitrary and equivalent formulas can be obtained with other choices⁸. Here, our choice is motivated by the fact that x^0 is the time at which the external source J turns off. In view of the resummation we will use later, it is important to note that the quantum field fluctuations β and $a_{\pm\mathbf{k}}$ are still small relative to the classical field at the splitting time used in the formula. That this is true in our case is transparent from the figure 2.

2.6 Resummation of the NLO corrections

As seen previously, the fixed order NLO calculation is not meaningful after a certain time, because it gives a pressure that is larger than the LO contribution. The NLO contribution (and likely any higher fixed loop order contribution) has secular divergences because it involves the *linearized* equation of motion for perturbations to the classical field φ . In other words, if $\psi \equiv \varphi + a$, the NLO calculation approximates the dynamics of ψ by

$$\begin{aligned} \square\varphi + V'(\varphi) &= J \\ \left[\square + V''(\varphi) \right] a &= 0, \end{aligned} \quad (18)$$

⁸The splitting of the time evolution in two halves need not be done at a constant x^0 and any locally space-like hypersurface will suffice.

on the grounds that the nonlinear terms in a are formally of higher order in g^2 . Obviously, if the dynamics of ψ was treated exactly, by solving instead⁹

$$\square\psi + V'(\psi) = J, \quad (19)$$

we would not have any divergence because the ψ^4 potential would prevent runaway growth of ψ . However, in order to achieve this substitution, we must include in our calculation some contributions that are of higher order in g^2 . Thus, we seek a resummation that restores the lost nonlinearity in the field fluctuations, while keeping in full the LO and NLO contributions that we have already calculated.

As we will argue in this section, a simple resummation that leads to an energy-momentum tensor which is finite at all times consists in starting from eq. (16) and in exponentiating the operator inside the square brackets,

$$T_{\text{resum}}^{\mu\nu}(x) \equiv \exp \left[\int d^3\mathbf{u} \beta \cdot \mathbb{T}_{\mathbf{u}} + \frac{1}{2} \int d^3\mathbf{u} d^3\mathbf{v} \int \frac{d^3\mathbf{k}}{(2\pi)^3 2k} [a_{+\mathbf{k}} \cdot \mathbb{T}_{\mathbf{u}}] [a_{-\mathbf{k}} \cdot \mathbb{T}_{\mathbf{v}}] \right] T_{\text{LO}}^{\mu\nu}(x), \quad (20)$$

If we Taylor expand the exponential, we recover the full expressions for the LO and NLO contributions, plus an infinite series of other terms that are of higher order in g^2 ,

$$T_{\text{resum}}^{\mu\nu}(x) = \frac{Q^4}{g^2} \left[\underbrace{c_0 + c_1 g^2}_{\text{fully}} + \underbrace{c_2 g^4 + \dots}_{\text{partly}} \right]. \quad (21)$$

From the form of eq. (20), it is not evident that the exponentiation leads to a better behaved result; on the surface it appears that we are including an infinite series of terms that are increasingly pathological at large times. To see that the result is now stable when $x^0 \rightarrow +\infty$, let us consider some generic function of the classical field at the point x , $\tilde{F}[\varphi(x)]$. The field $\varphi(x)$ is itself a functional of the values¹⁰ φ_0 of the field and $\dot{\varphi}_0$ of its first time derivative at $x^0 = 0$. Thus, the quantity $\tilde{F}[\varphi(x)]$ is implicitly a function of $\varphi_0, \dot{\varphi}_0$,

$$\tilde{F}[\varphi(x)] \equiv F[\varphi_0, \dot{\varphi}_0]. \quad (22)$$

Note now that the exponential of $\beta \cdot \mathbb{T}_{\mathbf{u}}$ is a translation operator when it acts on a functional $F[\varphi_0(\mathbf{u}), \dot{\varphi}_0(\mathbf{u})]$,

$$\exp \left[\int d^3\mathbf{u} \beta \cdot \mathbb{T}_{\mathbf{u}} \right] F[\varphi_0, \dot{\varphi}_0] = F[\varphi_0 + \beta, \dot{\varphi}_0 + \dot{\beta}]. \quad (23)$$

The first term in the exponential in eq. (20) therefore merely shifts the initial conditions $\varphi_0, \dot{\varphi}_0$ at $x^0 = 0$ of the classical field φ (by amounts $\beta, \dot{\beta}$). Similarly,

⁹Though this expression looks identical to the first equation of eq. (18), the initial conditions for this equation are different, leading to a different solution.

¹⁰Although we do not write that explicitly in order to simplify the notation, φ_0 and $\dot{\varphi}_0$ may depend on the position \mathbf{x} .

the second term, that involves the exponential of an operator that has two \mathbb{T} 's, can be rewritten as a sum over fluctuations of the initial classical field¹¹

$$\begin{aligned} \exp \left[\frac{1}{2} \int d^3 \mathbf{u} d^3 \mathbf{v} \int \frac{d^3 \mathbf{k}}{(2\pi)^3 2k} [a_{+\mathbf{k}} \cdot \mathbb{T}_{\mathbf{u}}] [a_{-\mathbf{k}} \cdot \mathbb{T}_{\mathbf{v}}] \right] F[\varphi_0, \dot{\varphi}_0] &= \\ &= \int [D\alpha D\dot{\alpha}] Z[\alpha, \dot{\alpha}] F[\varphi_0 + \alpha, \dot{\varphi}_0 + \dot{\alpha}], \end{aligned} \quad (24)$$

where the distribution $Z[\alpha, \dot{\alpha}]$ is Gaussian in $\alpha(\mathbf{x})$ and $\dot{\alpha}(\mathbf{x})$, with 2-point correlations given by

$$\begin{aligned} \langle \alpha(\mathbf{x}) \alpha(\mathbf{y}) \rangle &= \int \frac{d^3 \mathbf{k}}{(2\pi)^3 2k} a_{+\mathbf{k}}(0, \mathbf{x}) a_{-\mathbf{k}}(0, \mathbf{y}), \\ \langle \dot{\alpha}(\mathbf{x}) \dot{\alpha}(\mathbf{y}) \rangle &= \int \frac{d^3 \mathbf{k}}{(2\pi)^3 2k} \dot{a}_{+\mathbf{k}}(0, \mathbf{x}) \dot{a}_{-\mathbf{k}}(0, \mathbf{y}). \end{aligned} \quad (25)$$

Therefore, the energy-momentum tensor resulting from the resummation of eq. (20) can be written as

$$T_{\text{resum}}^{\mu\nu} = \int [D\alpha(\mathbf{x}) D\dot{\alpha}(\mathbf{x})] Z[\alpha, \dot{\alpha}] T_{\text{LO}}^{\mu\nu}[\varphi_0 + \beta + \alpha], \quad (26)$$

where $T_{\text{LO}}^{\mu\nu}[\varphi_0 + \beta + \alpha]$ denotes the LO energy-momentum tensor evaluated with a *classical field* whose initial condition at $x^0 = 0$ is $\varphi_0 + \beta + \alpha$ (and likewise for the first time derivative).

From eq. (26), one can now see why the proposed resummation cures the pathologies of the NLO contribution. While the fixed-order NLO result involved linearized perturbations to the classical fields (that are generically divergent when $x^0 \rightarrow \infty$), in the resummed expression these perturbations appear only as a shift of the initial condition for the full *non-linear equation of motion*. After this resummation, the evolution of the perturbations at $x^0 > 0$ is no longer linear—since the ϕ^4 potential is bounded from below the evolution is stable.

In addition to manifestly demonstrating the stable evolution demanded by the underlying theory, eq. (26) is a most useful expression for a practical implementation of our resummation. It is important to note however that the integral over \mathbf{k} in the 2-point correlations (eq. (25)) that define the Gaussian distribution of α and $\dot{\alpha}$ should be cut-off at a value $\Lambda \sim g\varphi_0 \sim Q$ in order to avoid ultraviolet singularities. With such a cutoff, one can show that the sensitivity to the value of the cutoff is of higher order in g^2 , while at the same time being large enough to include in the resummation all the relevant unstable modes (the modes with $Q \lesssim |\mathbf{k}|$ are all stable).

¹¹An elementary form of the identity,

$$e^{\frac{\gamma}{2} \partial_x^2} f(x) = \int_{-\infty}^{+\infty} dz \frac{e^{-z^2/2\gamma}}{\sqrt{2\pi\gamma}} f(x+z),$$

can be proven by doing a Taylor expansion of the exponential in the left hand side and of $f(x+z)$ in the right hand side. In this simple example, one sees that an operator which is Gaussian in derivatives is a *smearing operator* that amounts to convoluting the target function with a Gaussian. Another way of proving the formula is to apply a Fourier transform to both sides of the equation.

3 $T_{\text{resum}}^{\mu\nu}$ from spatially uniform fluctuations

Before we proceed to a full 3+1-dimensional numerical evaluation of eq. (26) with an *ab initio* computation of eq. (25), we shall first consider, as a warm-up exercise, a computation including only spatially homogeneous fluctuations. Albeit not realistic, this much simpler calculation will be very instructive in understanding the effects of these fluctuations on the behavior of the energy-momentum tensor.

3.1 Setup of the problem

For spatially homogeneous fluctuations, the main simplification is that functional integrations over the fields α and $\dot{\alpha}$ in eq. (26) become ordinary integrals over a pair of real numbers, with the Gaussian weight

$$Z(\alpha, \dot{\alpha}) \equiv \exp \left[- \left(\frac{\alpha^2}{2\sigma_1} + \frac{\dot{\alpha}^2}{2\sigma_2} \right) \right]. \quad (27)$$

The two parameters $\sigma_{1,2}$ can be used in this toy calculation to control the magnitude of the fluctuations. In the limit $\sigma_{1,2} \rightarrow 0$, we recover the leading order result which of course receives no contribution from the fluctuations.

The second important simplification in this toy calculation is that since both the underlying classical field and the fluctuations are spatially homogeneous, the field equation of motion is an ordinary differential equation¹². One should note that the characteristic oscillation frequency is directly proportional to the amplitude of $\varphi(t)$. This property of the solution will be key in interpreting the results that follow.

We now turn to the computation of the resummed pressure and energy density in this toy model. From eqs. (8) and (26), the expressions for the energy density and the pressure read

$$\begin{aligned} \epsilon_{\text{resum}} &= \left\langle \frac{1}{2} \dot{\varphi}^2 + V(\varphi) \right\rangle_{\alpha, \dot{\alpha}}, \\ p_{\text{resum}} &= \left\langle \frac{1}{2} \dot{\varphi}^2 - V(\varphi) \right\rangle_{\alpha, \dot{\alpha}}, \end{aligned} \quad (28)$$

¹²In this case, the field equations can even be solved analytically. This can be seen very simply: from energy conservation, $\frac{1}{2} \dot{\varphi}^2 + V(\varphi) = E_0 = V(\phi_{\text{max}})$ (with ϕ_{max} the amplitude of the oscillations of $\varphi(t)$), one gets

$$t = \text{const} + \frac{1}{\sqrt{2}} \int_0^{\varphi(t)} \frac{d\psi}{\sqrt{V(\phi_{\text{max}}) - V(\psi)}}.$$

For a ϕ^4 potential, the integral in the right hand side is an elliptic integral, and one can express $\varphi(t)$ as

$$\varphi(t) = \phi_{\text{max}} \text{cn}_{1/2}(g\phi_{\text{max}}t/\sqrt{24} + \text{const}),$$

where $\text{cn}_{1/2}$ is the Jacobi elliptic function of the first kind with the elliptic modulus $k = 1/2$. This expression is periodic with a period $T = 2\sqrt{24}K(1/2)/g\phi_{\text{max}}$, where $K(1/2) \approx 1.85$ is the complete elliptic integral of the first kind.

where φ is the solution of the classical equation of motion whose value at $x^0 = 0$ is $\varphi_0 + \alpha$ and whose time derivative at $x^0 = 0$ is $\dot{\varphi}_0 + \dot{\alpha}$. The brackets $\langle \dots \rangle_{\alpha, \dot{\alpha}}$ denote an averaging over all possible values of $\alpha, \dot{\alpha}$ with the distribution of eq. (27).

3.2 Energy momentum tensor

In fig. 4, we display the result of the toy model calculation in the limit where we do not have fluctuations ($\sigma_{1,2} \rightarrow 0$). As anticipated, the result is equivalent to the one displayed in fig. 1 for the leading order calculation. In this figure,

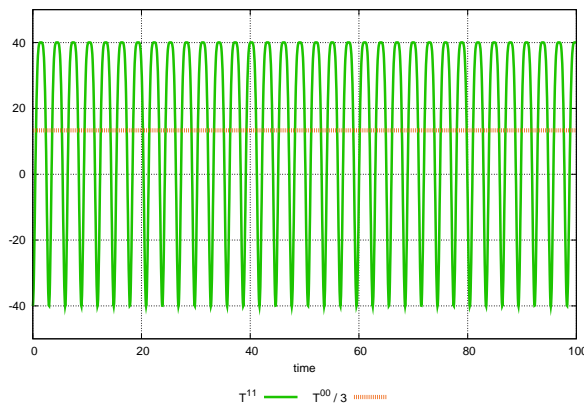


Figure 4: Components of $T_{LO}^{\mu\nu}$, where when no quantum fluctuations are included.

for reasons that will become obvious shortly, we have represented the energy density divided by three. In fig. 5, we show the results of the same calculation performed with non-zero widths $\sigma_{1,2}$ for the Gaussian distribution of fluctuations. We observe a striking difference of the resummed result compared to the previous (LO) figure—the oscillations of the pressure are damped and the value of the pressure relaxes to $\epsilon/3$. Subsequently, one has a single-valued relationship between the pressure and the energy density, namely, an *equation of state* – specifically, the equation of state $\epsilon = 3p$ of a scale invariant system in $1 + 3$ dimensions.

3.3 Phase-space density

It is also instructive to look at the phase-space density $\rho_t(\varphi, \dot{\varphi})$ of the points $(\varphi, \dot{\varphi})$ as the system evolves in time. This is shown in fig. 6. At $t = 0$, we start with a Gaussian distribution of the initial conditions, with a small dispersion around the average values ($\varphi = 10$ and $\dot{\varphi} = 0$ in our example).

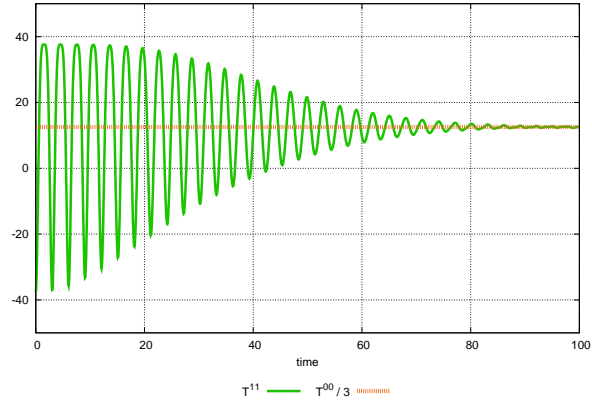


Figure 5: Components of $T_{\text{resum}}^{\mu\nu}$ obtained with a Gaussian ensemble of spatially uniform quantum fluctuations.

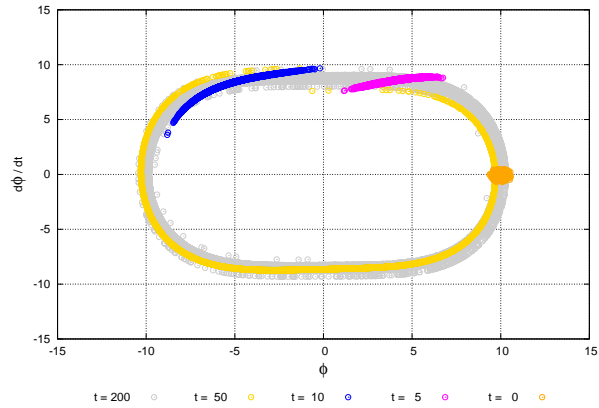


Figure 6: Phase-space distribution of the ensemble of classical fields at various stages of the time evolution.

Each initial condition then evolves independently according to the classical equation of motion, and the corresponding trajectory in the $(\varphi, \dot{\varphi})$ plane is a closed loop¹³ due to the periodicity of classical solutions. One observes that the initially Gaussian-shaped cloud of points starts spreading around a closed loop, to eventually fill it entirely when $x^0 \rightarrow +\infty$. When this asymptotic regime is reached, the density $\rho_t(\varphi, \dot{\varphi})$ depends only on the energy—roughly speaking, the radial coordinate in the plot of figure 6 and no longer on the angular coordinate.

A more formal way of phrasing the same result is to first note that the time evolution of the phase-space density ρ_t obeys the Liouville equation,

$$\frac{\partial \rho_t}{\partial t} + \{\rho_t, H\} = 0, \quad (29)$$

where $\{\cdot, \cdot\}$ is the classical Poisson bracket. Therefore, if a stationary distribution is reached at late times, it can only depend on φ and $\dot{\varphi}$ via $H(\varphi, \dot{\varphi})$. The asymptotic behavior of the phase-space density in our toy model is reminiscent of a micro-canonical equilibrium state, in which the phase-space density is uniform on a constant energy manifold¹⁴. In other words, all micro-states that have the same energy are equally likely.

3.4 Interpretation of the results

We shall now discuss the physical interpretation of our results, first discussing the decoherence of the temporal evolution of the fields and their time derivatives, and subsequently, the impact of decoherence on the relaxation of the pressure towards that of a scale invariant system.

3.4.1 Decoherence time

Of the previous numerical observations, the easiest to understand is the spreading of the phase-space density around a closed orbit. Because the oscillations are non-harmonic, the various points in the plot of figure 6 rotate at different speeds¹⁵; in a ϕ^4 potential, the outer points rotate faster than the inner ones. Therefore, as time increases, the cloud of points spreads more and more due to this effect.

One can estimate the time necessary for the cloud of points to spread over a complete orbit. This happens when the angular spread of the points reaches the value 2π . For one field configuration, this angular variable is, up to a phase that depends on the initial condition, $\theta = \omega t$, and the angular velocity ω depends

¹³These loops are constant energy curves $\frac{1}{2}\dot{\varphi}^2 + V(\varphi) = H$.

¹⁴It should be noted here that a spatially homogeneous field is very special regarding this issue; indeed, any non-linear system with a single degree of freedom is ergodic. This is not necessarily the case if there are more than one degrees of freedom, as is the case in a full fledged field theory.

¹⁵The assumption of a scale invariant theory simplifies some expressions here, but is not crucial to the argument. The only requirement for this phenomenon is that the frequency of the oscillations depends on their amplitude; thus any non-harmonic potential will lead to similar results.

only on the energy of that particular field configuration. (In our case, this phase is small for a narrow Gaussian distribution.) If we consider two field configurations, their angular variable difference $\Delta\theta$ increases linearly in time, $\Delta\theta = \Delta\omega t$, where $\Delta\omega$ is the difference between their angular velocities. In the case of a $g^2\phi^4/4!$ potential, one can prove that (see the footnote 12)

$$\omega = \frac{\pi}{2\sqrt{3}} \frac{g\phi_{\max}}{\int_{-1}^{+1} \frac{dx}{\sqrt{1-x^4}}} \approx 0.346 g\phi_{\max}, \quad (30)$$

where ϕ_{\max} is amplitude of the oscillations of the φ field. Thus, the angular shift between the two field configurations is also $\Delta\theta \approx 0.346 g\Delta\phi_{\max} t$, and this shift reaches 2π in a time

$$t \approx \frac{18.2}{g\Delta\phi_{\max}}. \quad (31)$$

After this time, the two fields have become completely incoherent. We see that this time is inversely proportional to the coupling constant g , and to the difference of the field amplitudes. Thus a narrow initial Gaussian distribution will need a longer time to spread around the orbit than a broader initial distribution.

3.4.2 Equation of state from quantum averaging

Once we know that the phase-space density spreads uniformly on constant energy curves, it is easy to understand why the pressure relaxes towards $\epsilon/3$ when we let the initial conditions for the classical field fluctuate. The trace of the energy-momentum tensor (assuming 4 dimensions of space-time) is

$$T^\mu{}_\mu = \varphi \left(\square\varphi + 4 \frac{V(\varphi)}{\varphi} \right) - \partial_\alpha(\varphi\partial^\alpha\varphi). \quad (32)$$

A scale invariant theory in four dimensions is a theory in which the interaction potential obeys $V'(\varphi) = 4V(\varphi)/\varphi$. This is the case of a ϕ^4 interaction. Therefore, the first term in the right hand side of the previous equation vanishes thanks to the equation of motion of the classical field φ . This result shows that the energy-momentum tensor of a single configuration of classical field is not zero in our model, but is a total derivative¹⁶. In our simplified toy model where the fields are spatially homogeneous, the previous relation simplifies to

$$T^\mu{}_\mu = -\frac{d(\varphi\dot{\varphi})}{dt}. \quad (33)$$

When averaged over one period, the trace of the energy-momentum of one classical field configuration vanishes because the classical field is a periodic function of time,

$$\overline{T^\mu{}_\mu} \equiv \frac{1}{T} \int_t^{t+T} d\tau T^\mu{}_\mu(\varphi(\tau), \dot{\varphi}(\tau)) = 0, \quad (34)$$

¹⁶There is an alternative “improved” definition of the energy-momentum tensor that is explicitly traceless [49]. However, while the energy density has a single valued relation to the pressure, this pressure is not the canonical pressure. As we shall discuss later in section 3.5.3, both definitions give a deviation from ideal hydrodynamic flow, which is cured by the quantum averaging described here.

where the result is independent of t . When we calculate the energy-momentum tensor averaged over fluctuations of the initial conditions, we are in fact performing an ensemble average weighted by the phase-space density $\rho_t(\varphi, \dot{\varphi})$,

$$\langle T^\mu{}_\mu \rangle_{\alpha, \dot{\alpha}} = \int d\varphi d\dot{\varphi} \rho_t(\varphi, \dot{\varphi}) T^\mu{}_\mu(\varphi, \dot{\varphi}) , \quad (35)$$

and the time dependence of the left hand side comes from that of the density ρ_t . It is convenient to trade the integration variables $\varphi, \dot{\varphi}$ for energy/angle variables E, θ ,

$$\langle T^\mu{}_\mu \rangle_{\alpha, \dot{\alpha}} = \int dE d\theta \tilde{\rho}_t(E, \theta) T^\mu{}_\mu(E, \theta) , \quad (36)$$

where $\tilde{\rho}_t$ is the phase-space density in the new system of coordinates¹⁷. Our first result shows that $\tilde{\rho}_t(E, \theta) \rightarrow \tilde{\rho}_t(E)$, namely, becomes independent of θ at late times, which enables us to write the previous equation as

$$\langle T^\mu{}_\mu \rangle_{\alpha, \dot{\alpha}} \underset{t \rightarrow \infty}{\approx} \int dE \tilde{\rho}_t(E) \int d\theta T^\mu{}_\mu(E, \theta) . \quad (37)$$

The crucial point here is that the integral over θ is simply the integral over one orbit for a single classical field configuration (eq. (34)),

$$\int d\theta T^\mu{}_\mu(E, \theta) = \frac{2\pi}{T} \int_t^{t+T} d\tau T^\mu{}_\mu(\varphi(\tau), \dot{\varphi}(\tau)) = 0 . \quad (38)$$

Thus, we have proven that

$$\epsilon - 3p = \langle T^\mu{}_\mu \rangle_{\alpha, \dot{\alpha}} \underset{t \rightarrow \infty}{\approx} 0 , \quad (39)$$

in agreement with what we have observed numerically. Moreover, from the derivation of this result, it is clear that the time necessary to reach this limit is the same as the time (in eq. (31)) necessary for the phase-space density to become independent of the angular variable θ .

3.5 Effect of the longitudinal expansion

We have thus far considered a system of strong fields enclosed in a box of fixed volume. There is therefore no concept of hydrodynamical flow in such a system. To fully understand the implications of decoherence and relaxation of the pressure we have discussed previously for hydrodynamical flow, we will now simply generalize the toy problem of spatially uniform fields and fluctuations to a system undergoing a boost invariant one dimensional expansion.

¹⁷ $\tilde{\rho}_t$ is equal to the original ρ_t times the Jacobian of the change of variables.

3.5.1 Relaxation of the pressure

The geometry of the one dimensional expansion (chosen to be the z direction) is appropriate to describe the collision of two projectiles (nuclei) at ultrarelativistic energies. The natural coordinates are the proper time τ and rapidity η defined by

$$\begin{aligned}\tau &\equiv \sqrt{t^2 - z^2}, \\ \eta &\equiv \frac{1}{2} \ln \left(\frac{t+z}{t-z} \right).\end{aligned}\tag{40}$$

In the spatial plane orthogonal to the z axis, the coordinates are denoted by \mathbf{x}_\perp . In this system of coordinates, the classical equation of motion for a field φ that depends only on proper time is

$$\ddot{\varphi} + \frac{1}{\tau} \dot{\varphi} + \frac{g^2}{6} \varphi^3 = 0,\tag{41}$$

where the dot now denotes a derivative with respect to τ . The analog of the toy problem we discussed previously in the first part of this section is to let the initial conditions of the field have Gaussian fluctuations $\alpha, \dot{\alpha}$ that are independent of η and \mathbf{x}_\perp .

The components of the energy-momentum tensor in this system of coordinates, averaged over the fluctuations of the initial conditions are

$$\begin{aligned}\epsilon \equiv T^{\tau\tau} &= \left\langle \frac{1}{2} \dot{\varphi}^2 + V(\varphi) \right\rangle_{\alpha, \dot{\alpha}}, \\ p \equiv T^{xx} = T^{yy} = \tau^2 T^{\eta\eta} &= \left\langle \frac{1}{2} \dot{\varphi}^2 - V(\varphi) \right\rangle_{\alpha, \dot{\alpha}}.\end{aligned}\tag{42}$$

As in the fixed volume case, we shall use the distribution of eq. (27) for $\alpha, \dot{\alpha}$. The result of this computation is shown in the figure 7. The dots represent the energy density divided by 3, and one observes that its time dependence is well described by a $\tau^{-4/3}$ decay characteristic of boost invariant flow in ideal relativistic hydrodynamics. If we do not include fluctuations of the initial conditions, we observe that the pressure oscillates between positive and negative values, with a decreasing envelope. Conversely, if we average over an ensemble of initial conditions, we see the oscillations of the pressure dampen quickly, ensuring that the pressure approaches one third of the energy density.

These results are in sharp contrast to what one obtains for a ϕ^2 potential. The results are shown in fig. 8. In this case, the fluctuations do not make the pressure converge to $T^{00}/3$, and the latter decreases as τ^{-1} instead of $\tau^{-4/3}$.

3.5.2 Interpretation of the results for expanding fields

From the equation of motion in eq. (41), we obtain

$$\begin{aligned}\frac{d\epsilon}{d\tau} &= \dot{\varphi} \left[\ddot{\varphi} + V'(\varphi) \right] = -\frac{1}{\tau} \dot{\varphi}^2 \\ &= -\frac{\epsilon + p}{\tau}.\end{aligned}\tag{43}$$

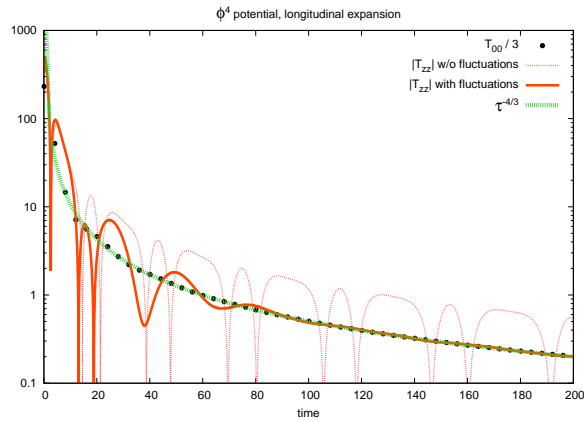


Figure 7: Numerical evaluation of $T^{\mu\nu}$ for fields undergoing a boost invariant 1-dimensional expansion in a ϕ^4 theory with a Gaussian ensemble of spatially uniform initial fluctuations.

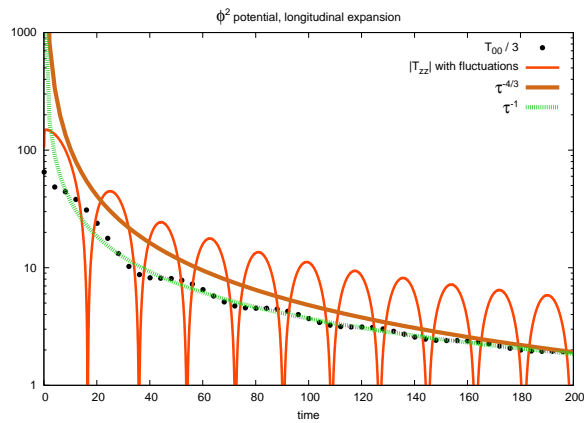


Figure 8: Numerical evaluation of $T^{\mu\nu}$ for fields undergoing a boost invariant 1-dimensional expansion in a ϕ^2 theory, with a Gaussian ensemble of uniform initial fluctuations.

This equation, which is valid for individual classical field configurations at every time, is identical to Euler's equation for boost-invariant ideal hydrodynamics. The difference with hydrodynamics lies in the fact that hydrodynamics assumes the existence of an equation of state $p = f(\epsilon)$ to ensure a closed form expression in eq (43). In classical field dynamics, one is not free to impose a relationship between ϵ and p since they are both completely determined from the field φ and its derivative $\dot{\varphi}$. For instance, as seen in fig. 7, for a single classical solution, we do not have a one-to-one correspondence between ϵ and p ; ϵ has a monotonous behavior while p oscillates. What is remarkable is that the ensemble average over the initial conditions leads in a short time to a one-to-one correspondence $\epsilon = 3p$, which is precisely the equation of state one would use in boost invariant hydrodynamics of a perfect fluid.

The mechanism whereby this relationship is reached is the same as in the non-expanding case. As previously, one can prove that for a single phase-space trajectory, the time averages of ϵ and p obey a relation identical to the expected equation of state, because the trace of the energy momentum tensor is a total derivative. Then, by using the fact that different initial conditions lead to different oscillation frequencies, one gets the phase decoherence that enables us to transform the ensemble average over the initial conditions into a time average along one classical field trajectory. This decoherence is the missing ingredient in the harmonic case—as we noted previously, it arises for the ϕ^4 theory because the angular velocity of the phase space trajectory of an individual configuration depends on the amplitude of the configuration.

From this result, it is very easy to obtain the $\tau^{-4/3}$ behavior of the energy density. The ensemble average of eq. (43) at late times is

$$\frac{d\epsilon}{d\tau} \Big|_{\tau \rightarrow +\infty} = -\frac{4}{3}\epsilon, \quad (44)$$

which leads immediately to the observed behavior. Since both ϵ and p decrease like $\tau^{-4/3}$ even for a single configuration (if one considers the envelope of the oscillations of p), this means that at late times we have

$$\varphi \sim \tau^{-1/3}, \quad \dot{\varphi} \sim \tau^{-2/3}. \quad (45)$$

This behavior is seen from the simple ansatz $\varphi(\tau) \sim \cos(f(\tau))\tau^{-1/3}$, which, while inaccurate in detail, qualitatively captures the right physics. For a φ^4 potential, the frequency $\dot{f} \propto \varphi \sim \tau^{-1/3}$ for a ϕ^4 potential; using this relation in our ansatz gives the stated result. The fact that $\dot{\varphi}$ decreases faster than φ is due to the slowing down of the oscillations with time, as their amplitude decreases.

3.5.3 Callan-Coleman-Jackiw energy-momentum tensor

An alternate definition of the energy-momentum tensor was proposed by Callan, Coleman and Jackiw (CCJ) [49]. Their expression is explicitly traceless. They argued further that their form of the stress energy tensor improved properties relative to the canonical one with regard to renormalization. Let us briefly

summarize the differences between the usual definition of $T^{\mu\nu}$ and CCJ's. With the canonical definition that we have used thus far, one has,

$$\begin{aligned}
T^{\mu\nu} &\equiv (\partial^\mu \varphi)(\partial^\nu \varphi) - g^{\mu\nu} \mathcal{L} \\
\epsilon &= \frac{1}{2} \dot{\varphi}^2 + V(\varphi) \\
p &= \frac{1}{2} \dot{\varphi}^2 - V(\varphi) \\
\epsilon - 3p &= \frac{d(\varphi \dot{\varphi})}{d\tau} \\
\frac{d\epsilon}{d\tau} &= -\frac{\epsilon + p}{\tau}.
\end{aligned} \tag{46}$$

With this definition of $T^{\mu\nu}$, one obtains the equation for Bjorken hydrodynamics automatically for each configuration of the classical field. However, one gets $\epsilon = 3p$ only through decoherence, by averaging over an ensemble of initial conditions.

In comparison, with CCJ's definition of the energy-momentum tensor, one has

$$\begin{aligned}
T^{\mu\nu} &\equiv (\partial^\mu \varphi)(\partial^\nu \varphi) - g^{\mu\nu} \mathcal{L} - \frac{1}{6}(\partial^\mu \partial^\nu - g^{\mu\nu} \square) \varphi^2 \\
\epsilon &= \frac{1}{2} \dot{\varphi}^2 + V(\varphi) \\
p &= \frac{1}{2} \dot{\varphi}^2 - V(\varphi) - \frac{1}{6} \square \varphi^2 \\
\epsilon - 3p &= 0 \\
\frac{d\epsilon}{d\tau} &= -\frac{\epsilon + p}{\tau} - \frac{1}{3\tau} \frac{d(\varphi \dot{\varphi})}{d\tau}.
\end{aligned} \tag{47}$$

With this form of the energy momentum tensor, the equation of state is satisfied for each classical field configuration, but not Bjorken's hydrodynamic equation. It is only after an average over an ensemble of initial conditions that the last term ($\sim d(\varphi \dot{\varphi})/d\tau$) in the last equation vanishes by decoherence.

Since one requires simultaneously

$$\begin{aligned}
\frac{d\epsilon}{d\tau} + \frac{\epsilon + p}{\tau} &= 0 \\
\epsilon - 3p &= 0,
\end{aligned} \tag{48}$$

for ideal hydrodynamical flow, one sees that there is no discrepancy between the two descriptions despite the apparent differences. For our choice of the energy momentum tensor, the reason why we didn't have an ideal hydrodynamic behavior at the beginning of the evolution was because of the lack of an equation of state. In the case of CCJ's energy momentum tensor, it is because of a violation of the canonical Euler equation. The net effect of the quantum averaging in each case is to get rid of one or the other violation thereby ensuring ideal hydrodynamical behavior. In the following section, we will discuss only the canonical energy momentum tensor, for which the focus is on obtaining the equation of state as the necessary condition for hydrodynamical flow.

4 Results from the full fluctuation spectrum

In the previous section, we showed that averaging over an ensemble of initial conditions for classical fields can lead the pressure to relax towards one third of the energy density. However, this study was oversimplified since we used only fluctuations that are uniform in space, and their Gaussian distribution was set by hand. However, quantum field theory *predicts* what the spectrum of these fluctuations is: one should average the LO energy-momentum tensor¹⁸,

$$T_{\text{resum}}^{\mu\nu} = \langle T_{\text{LO}}^{\mu\nu}[\varphi_0 + \alpha] \rangle_{\alpha, \dot{\alpha}}, \quad (49)$$

over space-dependent random Gaussian fields α and $\dot{\alpha}$ that have the following variance:

$$\begin{aligned} \langle \alpha(\mathbf{x})\alpha(\mathbf{y}) \rangle &= \int \frac{d^3\mathbf{k}}{(2\pi)^3 2k} a_{+\mathbf{k}}(0, \mathbf{x}) a_{-\mathbf{k}}(0, \mathbf{y}) \\ \langle \dot{\alpha}(\mathbf{x})\dot{\alpha}(\mathbf{y}) \rangle &= \int \frac{d^3\mathbf{k}}{(2\pi)^3 2k} \dot{a}_{+\mathbf{k}}(0, \mathbf{x}) \dot{a}_{-\mathbf{k}}(0, \mathbf{y}), \end{aligned} \quad (50)$$

which leaves no freedom to handpick what fluctuations we use. From these formulas, we can numerically compute *ab initio* the behavior of the pressure. The only tunable quantities in the calculation are then the scale Q (or more generally the source J) that controls the amount of energy injected into the system at $t < 0$, and the coupling constant g . Note that the above spectrum of fluctuations for the initial condition for the field φ is equivalent to parameterizing the initial field as¹⁹

$$\varphi(0, \mathbf{x}) \equiv \varphi_0(0, \mathbf{x}) + \int \frac{d^3\mathbf{k}}{(2\pi)^3 2k} \left[c_{\mathbf{k}} a_{+\mathbf{k}}(0, \mathbf{x}) + c_{\mathbf{k}}^* a_{-\mathbf{k}}(0, \mathbf{x}) \right], \quad (51)$$

where the $c_{\mathbf{k}}$ are random Gaussian numbers with the following variance

$$\langle c_{\mathbf{k}} c_{\mathbf{l}} \rangle = 0, \quad \langle c_{\mathbf{k}} c_{\mathbf{l}}^* \rangle = (2\pi)^3 |\mathbf{k}| \delta(\mathbf{k} - \mathbf{l}). \quad (52)$$

Details of the numerical lattice computation are relegated to the appendix A; in this section we focus on the results from numerical simulations with this *ab initio* spectrum of fluctuations.

4.1 Numerical results

Unless stated otherwise, the numerical results in this section are obtained on a 12^3 lattice²⁰. The functional integration in eq. (26) is approximated by a Monte-Carlo average over 1000 configurations of the initial conditions, distributed according to eqs. (51) and (52).

¹⁸Since, at $x^0 = 0$, β (see eq. (26)) is a small shift that does not fluctuate, we have absorbed it into a redefinition of the classical field φ_0 .

¹⁹If we recall that the $a_{\pm\mathbf{k}}$'s are plane waves modified by the presence of the background field φ_0 , we observe that the fluctuating part of the initial field is very similar to the form of the wavefunction of high lying eigenstates for quantum systems that obey Berry's conjecture.

²⁰In some instances, we have also performed simulations on a 20^3 lattice and found only very small differences as long as the physical scales are below the lattice cutoff.

In fig. 9, we show the result of the computation of the pressure averaged over the Gaussian ensemble of initial conditions, for a value of the coupling²¹ $g = 0.5$. We also show the energy density divided by three on the same plot. All the quantities in this plot are expressed in lattice units, which means that

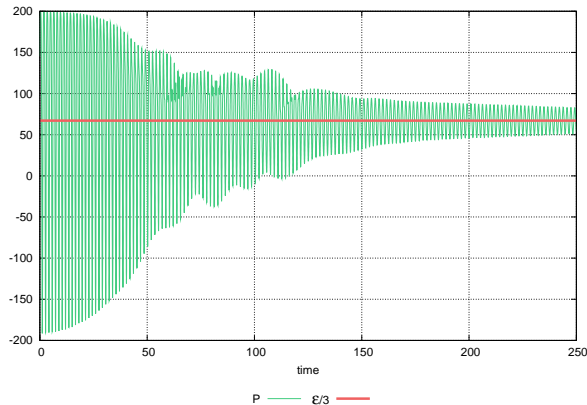


Figure 9: Time evolution of the pressure averaged over the initial fluctuations. All the resonant modes are included in the simulation. The coupling constant is $g = 0.5$.

the horizontal axis is t/a (where a is the lattice spacing) and the vertical axis should be understood as $\epsilon a^4/3$ or pa^4 . The lattice cutoff in this simulation is chosen to be just above the upper limit of the parametric resonance window ($k/m_0 = 3^{-1/4}$ where $m_0^2 = g^2\varphi_0^2/2$); therefore, all the resonant modes take part in the dynamics of the system.

We observe that the ensemble averaged pressure relaxes towards $\epsilon/3$. This plot, obtained with the spectrum of fluctuations predicted by quantum field theory, is one of the central results of this paper. One can qualitatively identify two stages in this relaxation: (1) in the range $0 \leq t \lesssim 50$, the amplitude of the pressure oscillations decreases very quickly to a moderate value and, (2) from time 50 onwards, one has a slower approach of the pressure to $\epsilon/3$ that gets slowly rid of the residual oscillations. We will observe again this two-stage time evolution when we look at the fluctuations of the energy density.

4.2 Influence of the resonant modes

In section 3, we observed that the pressure relaxes to $\epsilon/3$ even if only the mode $\mathbf{k} = 0$ is included in the simulation. This was understood as a consequence of the phase decoherence that exists in a non-harmonic potential between classical solutions that have slightly different amplitudes. When we include all the

²¹Since the prefactor in the interaction potential is $g^2/4!$, a value $g = 0.5$ corresponds to a very weak coupling strength.

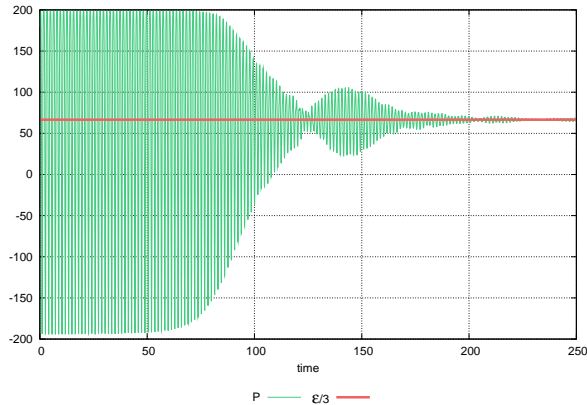


Figure 10: Time evolution of the pressure averaged over the initial fluctuations. The lattice cutoff is located below the resonance band in order to exclude them from the simulation. The coupling constant is $g = 0.5$.

\mathbf{k} -modes of the fluctuations, the situation becomes more complicated. In particular, the stability analysis of these fluctuations (see the appendix B) indicates that in addition to a linear instability of the soft modes due to the above mentioned decoherence phenomenon, there are also exponentially unstable modes in a narrow band of values \mathbf{k} .

In order to assess the role played in the time evolution by the modes of the resonance band, we performed a second simulation with the same physical parameters, but now with the lattice cutoff placed just below the lower end of the resonance band. This makes certain that none of the modes that exist on this lattice has an exponential instability. Since the resonance band is quite narrow, this is a small change of the cutoff in physical units because the cutoff in the earlier simulation was just above the upper end of the resonance band. However, one can see in the figure 10 that excluding the resonant modes leads to significant changes.

The final outcome, the relaxation of the pressure towards $\epsilon/3$, is not changed, but the details of the time evolution of the pressure are modified. Firstly, one observes a rather long delay during which the oscillations of the pressure remain almost constant in amplitude. Then, at a time of order 75 in lattice units, these oscillations are damped very quickly to very small wiggles around $\epsilon/3$. Except for a brief relapse, the oscillations remain very small after this time. In particular, the two-stage evolution that we observed with the full spectrum is now replaced by the following two stages: (1) nothing happens and, (2) very rapid relaxation that leaves almost no residual oscillations.

Therefore, it appears that the resonant modes, even if their presence or absence in the resummation does not change the final outcome, do alter significantly the detailed time evolution of the pressure. At this point, the precise

role of the resonant modes is somewhat unclear. It appears that the dynamics of the complete system is much richer than what one can learn by studying the linearized evolution of a single mode as done in the stability analysis of the appendix B. This analysis does not capture the non-linear couplings between the various modes (once the instabilities have made them large) which gives them a big role in the late stage evolution of the system. This certainly deserves further study.

4.3 Dependence on the coupling constant

The simulation that led to the result of fig. 9 was performed with a value $g = 0.5$ for the coupling constant – a very small value for our scalar field theory since there is also a factor $1/4!$ in the interaction potential. We have studied the time

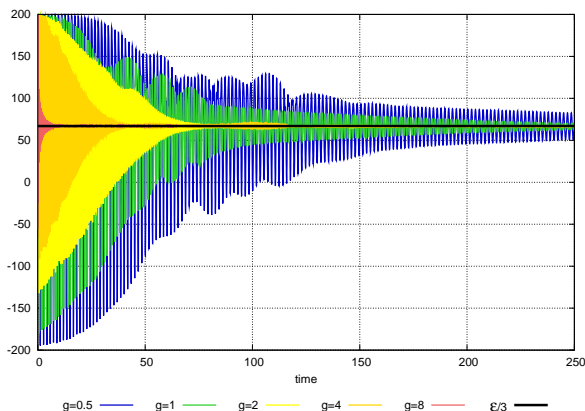


Figure 11: Time evolution of the pressure averaged over the initial fluctuations for various values of the coupling constant: $g = 0.5, 1, 2, 4, 8$. All the resonant modes are included in the simulation. See footnote 22.

evolution of the pressure for larger values of the coupling constant: $g = 1, 2, 4, 8$, and the results are shown in the figure 11. Note that this computation is done at fixed energy density. Indeed, because Q is the only dimensionful parameter of our model and there is a factor $1/g$ in the source J , the energy density behaves at leading order as $\epsilon \propto Q^4/g^2$. Thus, if we increase g at constant Q , the energy density decreases. As our goal is to assess the time at which the pressure obeys an equation of state (thereby justifying a hydrodynamical description of the system), the comparison of the relaxation for various couplings should be done for systems that have the same energy density. Therefore, in the comparison shown in fig. 11, the value of Q has been adjusted in each simulation such that the energy density remains unchanged.

Fig. 11 demonstrates that the relaxation time decreases with increasing coupling constant g . In fig. 12 we have represented the relaxation time, defined

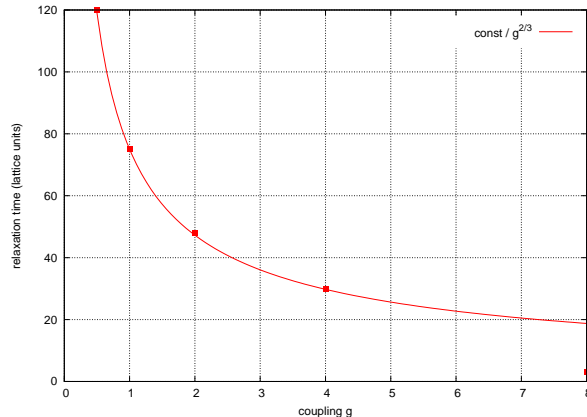


Figure 12: Points: relaxation time (see text for the definition used here) as a function of the coupling g . Line: fit by a power law.

here as the time necessary to reduce the initial oscillations of the pressure by a factor 4, as a function of the coupling constant g for our set of values of g . One can fit all the points except the last one ($g = 8$) by a power law that suggests the following dependence²²

$$t_{\text{relax}} = \frac{\text{const}}{g^{2/3}\epsilon^{1/4}}. \quad (53)$$

The right most point in this plot is an outlier that does not follow this power law, possibly because this value of the coupling is too extreme for our approximations/resummations to make sense (for $g = 8$, the interaction strength $g^2/4!$ is significantly above 1).

4.4 Energy density fluctuations

The results we have shown thus far indicate that the pressure in the system relaxes towards the equation of state $p = \epsilon/3$, at relaxation times that decrease as the coupling constant increases. However, this study does not in and of itself tell us much about the nature of the state reached by the system. In particular, it does not tell us whether the system reaches a state of local thermal equilibrium. Because we have a system of strong fields whose modes have large occupation numbers, it is unlikely that the system can be described in terms of quasi-particles that have a Bose-Einstein distribution. In section 3, we observed that

²²The axis of the figure 11 are in lattice units. Thus, the horizontal axis is t/a and the vertical axis pa^4 or $\epsilon a^4/3$, where a is the lattice spacing. Since our model is scale invariant, the relaxation time scales like $\epsilon^{-1/4}$. By eliminating a between the horizontal and vertical axis, it is easy to get the value of $\epsilon^{1/4}t$. For $g = 4$ we have $\epsilon a^4 = 200$ and the relaxation time is $t/a \approx 30$, leading to $\epsilon^{1/4}t \approx 113$ (this combination is 11 for $g = 8$). Then, from one's favorite value of ϵ in GeV/fm³, it is easy to obtain the relaxation time in fm's.

in the simple example studied that the phase-space density reaches a stationary form reminiscent of a micro-canonical equilibrium ensemble. Unfortunately, now that we are looking at a full fledged quantum field theory, the phase-space is infinite dimensional and whether the same behavior occurs is difficult to assess numerically.

There are however signs of thermalization in the fluctuations of the energy distribution in the system. For the system as a whole, energy is conserved and will not fluctuate, regardless of whether the system is in thermal equilibrium or not. However, as is well known for canonical ensembles, by looking at energy fluctuations in a small subsystem, one can learn something about the energy exchanges between this subsystem and the rest of the system which acts as a heat bath. In particular, the nature of the fluctuations in the energy distribution of the subsystem can tell us whether it is in equilibrium with the rest of the system. If this is the case, the fluctuations are those of a canonical ensemble with a density operator $\rho \equiv \exp(-\beta H)$.

We show in figs. 13 and 14 results from a study for the smallest subsystem one can conceive of on a lattice—a single lattice site. In fig. 13, we display histograms

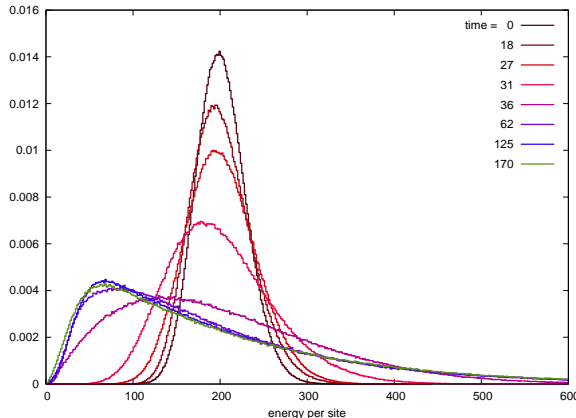


Figure 13: Distribution of energy density at one lattice site, at various times in the evolution. The coupling constant is $g = 0.5$.

of the values of the energy on one site²³, at various times in the evolution. These curves are normalized so that their integral is unity—they can be interpreted as probability distributions for the value of the energy on one lattice site. At $t = 0$, this distribution is very close to a Gaussian, centered on the mean energy density in the system. The width of this Gaussian is entirely determined by the Gaussian spectrum of fluctuations in eq. (25). At early times, the distribution first remains Gaussian-like, but tends to broaden with time. Around $t \approx 30$ in lattice units, we observe a rapid change of shape of this distribution—the peak of the distribution shifts to lower values of the energy and the tail extends much

²³In lattice units, this is simply the value of T^{00} at one given site.

further at large energy. Once this dramatic change of shape has taken place, the evolution of the distribution is rather slow and a stationary distribution is reached at late times.

The evolution in the energy distribution can be explored further by looking at its moments defined by

$$C_n \equiv \frac{\langle E^n \rangle}{\langle E \rangle^n}. \quad (54)$$

Higher moments are very sensitive to changes in the shape of the distribution, especially the appearance of an extended tail that signals broader energy fluctuations. We represent these moments as a function of time in fig. 14, up to

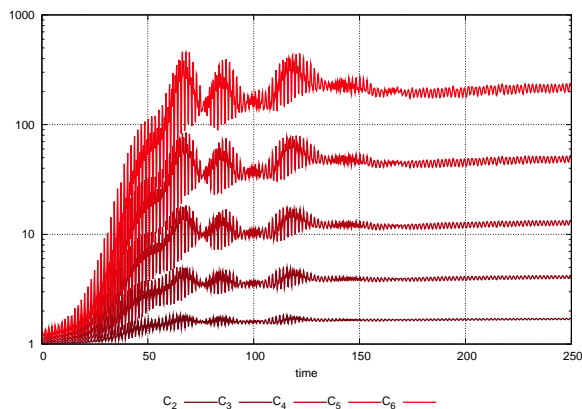


Figure 14: Normalized moments $\langle E^n \rangle / \langle E \rangle^n$ of the energy density distribution at one lattice site, as a function of time. The coupling constant is $g = 0.5$.

$n = 6$. They all start very close to 1 at $t = 0$, which is the sign of a very narrow distribution with little fluctuations. The rapid change of shape of the distribution around $t \approx 30$ corresponds to a rapid increase of the moments. By $t \approx 70$, the moments have reached nearly asymptotic values modulo moderate residual oscillations.

It is interesting to compare the evolution of the energy distribution at a single lattice site with the time evolution of the pressure in fig. 9. The initial rapid decrease of the pressure oscillations is concomitant with the change of shape of the energy distribution. The subsequent (slower) relaxation of the residual oscillations of the pressure occurs after the energy has reached a stationary distribution.

5 Summary and Outlook

We discussed in this paper a formalism which resums secular terms in a weak coupling expansion of a scalar field theory with initial conditions generated by

strong sources. We showed that resummed expressions, to all orders in perturbation theory, for inclusive quantities could be expressed as an ensemble average of the corresponding leading order classical quantities where the initial classical field for each member of the ensemble is shifted by a quantum fluctuation drawn from a Gaussian distribution. We showed that this averaging caused the resummed pressure to relax to a single valued relation with the energy density and interpreted this as arising from the phase decoherence of individual classical trajectories. We showed in a toy model that for an expanding system our result leads to ideal hydrodynamical flow. We briefly addressed the issue of thermalization—while our numerical results display features similar to those of a canonical thermal ensemble, they differ slightly in the particulars. A more systematic numerical study will likely be able to shed further light on this important point. As noted in the introduction, our system appears to satisfy Berry’s conjecture which has been argued to be an important requirement for the thermalization of quantum systems. We plan to pursue this topic further in the future.

Finally, we note that to be fully relevant to heavy ion collisions, our methods should be extended to gauge theories. We have shown previously that the formalism outlined in section 2 here is also applicable to a gauge theory [50]. The spectrum of quantum fluctuations [51] is the essential ingredient here and work on computing this quantity is well underway [52].

Acknowledgements

We would like to acknowledge useful discussions with Jean-Paul Blaizot, Kenji Fukushima, Miklos Gyulassy, Tuomas Lappi, Larry McLerran, Rob Pisarski, Andreas Schafer and Giorgio Torrieri. K.D’s and R.V’s research was supported by DOE Contract No. DE-AC02-98CH10886. F.G’s work is supported in part by Agence Nationale de la Recherche via the programme ANR-06-BLAN-0285-01. We thank the Institute for Nuclear Theory at the University of Washington for its hospitality. One of us (FG) would like to thank Brookhaven National Laboratory as well as the Yukawa International Program for Quark-Hadron Sciences at Yukawa Institute for Theoretical Physics (Kyoto University) for partial support during the completion of this work.

A Lattice implementation

In our numerical calculation, we discretize space in a L^3 cubic lattice, while retaining time as a continuous variable. This means that when solving the classical equation of motion for the field, the timestep is freely adjustable in order to warranty a given accuracy. In this appendix, we summarize the main aspects of this lattice formulation.

A.1 Discretization of space

The field $\varphi(t, \mathbf{x})$ (and its time derivatives) become a function of a continuous time t and of discrete indices i, j, k that vary between 0 and $L - 1$. We impose periodic spatial boundary conditions to the fields. In order to keep the code simple, all the dimensionful quantities are expressed in lattice units, which amounts to choosing a lattice spacing $a = 1$. Thus, the classical equation of motion for the field becomes:

$$\begin{aligned} \ddot{\varphi}_{ijk}(t) = & \varphi_{i+1jk} + \varphi_{i-1jk} + \varphi_{ij+1k} + \varphi_{ij-1k} + \varphi_{ijk+1} + \varphi_{ijk-1} - 6\varphi_{ijk} \\ & - \frac{g^2}{6}\varphi_{ijk}^3(t) + J_{ijk}(t). \end{aligned} \quad (55)$$

(The terms on the right hand side of the first line correspond to the discretized version of the Laplacian of the field.)

In our discretized description, there is an exactly conserved energy at $x^0 > 0$. To see that, multiply the previous equation by $\dot{\varphi}_{ijk}$ and sum over all the lattice sites,

$$\begin{aligned} \frac{d}{dt} \sum_{ijk} \left[\frac{1}{2} \dot{\varphi}_{ijk}^2 + \frac{1}{2} (\varphi_{i+1jk} - \varphi_{ijk})^2 + \frac{1}{2} (\varphi_{ij+1k} - \varphi_{ijk})^2 + \frac{1}{2} (\varphi_{ijk+1} - \varphi_{ijk})^2 \right. \\ \left. + \frac{g^2}{4!} \varphi_{ijk}^4 \right] = \sum_{ijk} J_{ijk} \dot{\varphi}_{ijk}. \end{aligned} \quad (56)$$

The left hand side of this equation, which is nothing but the time derivative of the total lattice energy, is zero when the source J is turned off. But note that for this to work, we had to use a non-symmetric form of the discrete derivative in the definition of the kinetic energy. Taking the seemingly more natural $\frac{1}{2}(\varphi_{i+1jk} - \varphi_{i-1jk})$ instead of $\varphi_{i+1jk} - \varphi_{ijk}$ would lead to an energy which is not exactly conserved on the lattice (though violations of energy conservation would be of higher order in the lattice spacing, it is preferable to use a lattice definition that makes it exactly conserved for any lattice spacing).

A.2 Small field fluctuations

To obtain the spectrum of fluctuations for the initial condition of the classical field, we must also consider the time evolution from $t = -\infty$ to $t = 0$ of small perturbations to the classical field that behave like plane waves in the remote past. On the lattice, free plane waves are labelled by three integers l, m, n and are of the form:

$$a_{ijk}^{(\pm lmn)}(t) \equiv e^{\pm i E_{lmn} t} e^{\mp \frac{2i\pi}{L}(il+jm+kn)}, \quad (57)$$

where the energy of the mode lmn is given by

$$E_{lmn} = \left[2 \left(3 - \cos\left(\frac{2\pi l}{L}\right) - \cos\left(\frac{2\pi m}{L}\right) - \cos\left(\frac{2\pi n}{L}\right) \right) \right]^{1/2}. \quad (58)$$

These plane waves obey the lattice Klein-Gordon equation,

$$\ddot{a}_{ijk} = a_{i+1jk} + a_{i-1jk} + a_{ij+1k} + a_{ij-1k} + a_{ijk+1} + a_{ijk-1} - 6a_{ijk} . \quad (59)$$

The lattice version of the fluctuations $a_{\pm\mathbf{k}}(x)$ that enter in eqs. (25) are fluctuations $a_{ijk}^{(\pm lmn)}(t)$ that obey

$$\begin{aligned} \ddot{a}_{ijk} + \frac{g^2}{2} \varphi_{ijk}^2 a_{ijk} &= \\ &= a_{i+1jk} + a_{i-1jk} + a_{ij+1k} + a_{ij-1k} + a_{ijk+1} + a_{ijk-1} - 6a_{ijk} \end{aligned} \quad (60)$$

and behave like the free waves of eq. (57) when $t \rightarrow -\infty$.

A.3 Sampling of the Gaussian fluctuations

Once the fluctuations that obey this equation and initial conditions are known, the discrete version of eq. (25) reads

$$\langle a_{ijk} a_{i'j'k'} \rangle = \frac{1}{L^3} \sum_{lmn} \frac{1}{2E_{lmn}} a_{ijk}^{(+lmn)}(0) a_{i'j'k'}^{(-lmn)}(0) , \quad (61)$$

and similar formulas for the correlators involving the time derivatives. Generating Gaussian fluctuations that have a given correlation function in general requires to diagonalize the 2-point correlator. On the lattice, this means that one should diagonalize an $L^3 \times L^3$ matrix, a fairly time consuming step even for a reasonably sized lattice.

In the case of the correlation function (61), it turns out that we can avoid this diagonalization. First of all, let us decompose a fluctuation a_{ijk} on the basis formed by the $a_{ijk}^{(\pm lmn)}$,

$$a_{ijk} \equiv \frac{1}{L^3} \sum_{lmn} \frac{1}{2E_{lmn}} \left[\alpha_{lmn} a_{ijk}^{(+lmn)} + \beta_{lmn} a_{ijk}^{(-lmn)} \right] . \quad (62)$$

Since we want to obtain a real field, we must have $\beta_{lmn} = \alpha_{lmn}^*$. Since there is a linear relation between a_{ijk} and the coefficients $\alpha_{lmn}, \beta_{lmn}$, it is obvious that these coefficients should also be Gaussian distributed. A little guesswork indicates that in order to obtain eq. (61), one needs

$$\begin{aligned} \langle \alpha_{lmn} \alpha_{l'm'n'} \rangle &= \langle \beta_{lmn} \beta_{l'm'n'} \rangle = 0 , \\ \langle \alpha_{lmn} \beta_{l'm'n'} \rangle &= E_{lmn} L^3 \delta_{ll'} \delta_{mm'} \delta_{nn'} . \end{aligned} \quad (63)$$

Equivalently, this can be translated into correlators for the real and imaginary parts of α_{lmn} :

$$\begin{aligned} \langle \text{Re}(\alpha_{lmn}) \text{Re}(\alpha_{l'm'n'}) \rangle &= \langle \text{Im}(\alpha_{lmn}) \text{Im}(\alpha_{l'm'n'}) \rangle = \frac{E_{lmn}}{2} L^3 \delta_{ll'} \delta_{mm'} \delta_{nn'} \\ \langle \text{Re}(\alpha_{lmn}) \text{Im}(\alpha_{l'm'n'}) \rangle &= 0 . \end{aligned} \quad (64)$$

In words, the real and imaginary parts of the coefficient α_{lmn} are independent Gaussian random variables. This leads to a straightforward algorithm for generating the correct Gaussian fluctuations of the initial conditions of the classical field:

- i.** From $t = -\infty$ (in practice, some large negative time) to $t = 0$, solve the classical equation of motion (55) for the classical field φ given a source J ,
- ii.** For each Fourier mode lmn , solve the equation of motion (60) for the small fluctuation $a^{(+lmn)}$, until $t = 0$,
- iii.** For each mode lmn , generate two random numbers $\text{Re}(\alpha_{lmn})$, $\text{Im}(\alpha_{lmn})$ drawn from a Gaussian distribution of variance $E_{lmn}L^3/2$,
- iv.** Construct a field fluctuation a, \dot{a} as

$$\begin{aligned} a_{ijk} &\equiv \frac{1}{L^3} \sum_{lmn} \frac{1}{E_{lmn}} \text{Re} \left[\alpha_{lmn} a_{ijk}^{(+lmn)}(0) \right], \\ \dot{a}_{ijk} &\equiv \frac{1}{L^3} \sum_{lmn} \frac{1}{E_{lmn}} \text{Re} \left[\alpha_{lmn} \dot{a}_{ijk}^{(+lmn)}(0) \right], \end{aligned} \quad (65)$$

and superimpose it on to the field $\varphi_{ijk}(0), \dot{\varphi}_{ijk}(0)$ in order to obtain a fluctuating initial condition for the evolution at $t > 0$. Repeat steps **iii** and **iv** for each configuration in the Monte-Carlo evaluation of eq. (26) in order to obtain an ensemble of initial conditions for the classical field.

- v.** For each initial condition constructed in this way, solve the classical equation of motion (55) for $t > 0$ (but now with $J = 0$). Compute the energy-momentum tensor of this classical field. Average it over the ensemble of initial conditions.

A.4 Ultraviolet sector

The summation over fluctuations of the initial conditions for the classical field in eq. (26), if performed without any constraint on the momentum of the fluctuations one includes, leads to ultraviolet divergences in the energy-momentum tensor.

For instance, if we impose a cutoff Λ on the momentum of the fluctuations included in eq. (26), one can check that generically the energy density will contain terms of the form

$$\epsilon = \frac{Q^4}{g^2} \oplus Q^2 \Lambda^2 \oplus \Lambda^4, \quad (66)$$

where Q is the physical scale introduced via the source J . Eq. (26) is not renormalizable in the usual sense, because it results from a resummation that mixes diagrams with arbitrarily high loop orders, and it should be seen as an effective formula that only makes sense with an ultraviolet cutoff. In order to

include all the Fourier modes that are subject to instabilities, we must choose the cutoff such that $Q \lesssim \Lambda$. On the other hand, the cutoff should not be too large, otherwise the result of eq. (26) will be cutoff dependent. It turns out that at weak coupling ($g \ll 1$), there is ample room to choose such a cutoff (large enough to encompass the relevant physics and small enough to keep the cutoff-dependent terms small). Indeed, it is sufficient to have

$$Q \lesssim \Lambda \ll \frac{Q}{\sqrt{g}}. \quad (67)$$

This window of allowed Λ 's can be enlarged if we notice that the Λ^4 terms are pure vacuum contributions, that can be computed and subtracted once for all²⁴. After this subtraction has been performed, the condition on Λ becomes

$$Q \lesssim \Lambda \ll \frac{Q}{g}. \quad (68)$$

Thus, taking Λ of order Q is a valid choice at small coupling.

A.5 Choice of the lattice cutoff

We have seen in the previous subsection that a UV cutoff is necessary in order to ensure the finiteness of eq. (26). One should choose the cutoff so that all the modes up to the resonance band are comprised below the cutoff. We have also seen that if the coupling constant is small, then the dependence on such a cutoff is negligible since it occurs only in terms that are subleading by one power of g^2 .

Such a cutoff exists naturally on the lattice, as a consequence of the discretization. In the figure 15, we have represented the density of lattice Fourier modes as a function of their energy E_{lmn} . This density falls abruptly when the energy reaches its maximal allowed value $E = \sqrt{12}$ (in lattice units), and no Fourier mode with a larger energy can exist on the lattice.

In lattice units ($a \equiv 1$), the interplay between the physical scales and the lattice cutoff can be tuned by adjusting the parameter Q that sets the magnitude of the source J . The modes that are the most important for the decoherence responsible for the relaxation towards the equation of state are the modes $k \lesssim Q$. If we chose a too large value of Q , the lattice cutoff will suppress modes that are important for this relaxation process. On the other hand, if Q is too low, then the physically relevant modes fall in the region where the density of lattice modes (see the figure 15) is very small. In this case, very few lattice modes are available to represent the relevant physics. The optimal choice of Q is to take it so that the resonance band is located just before the fall off of the mode density at large E_{lmn} . In this way, the physically relevant modes sit in the region where the lattice mode density is the largest.

²⁴This is done by running the same simulation with the source J turned off, and by subtracting the corresponding result. We find that on a 12^3 lattice, the vacuum contribution to T^{00} is almost independent of the coupling g , and equal to $T_{\text{vac}}^{00} \approx 1.35$. The vacuum contribution to the pressure tensor is proportional to the identity, with a pressure equal to $\frac{1}{3}T_{\text{vac}}^{00}$.

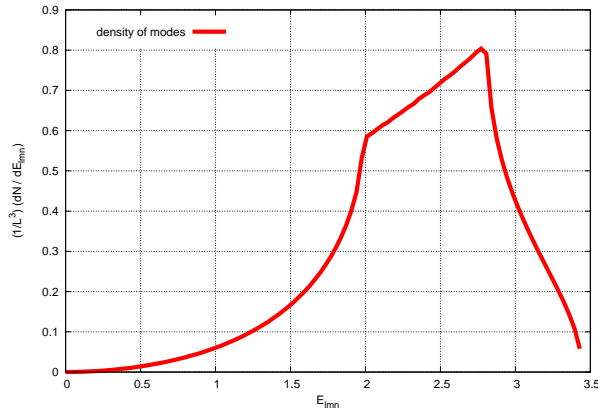


Figure 15: Density of Fourier modes as a function of their lattice energy (in the limit $L \rightarrow \infty$).

B Linear stability analysis for ϕ^4 field theory

B.1 Instabilities of small perturbations

The assumed g^2 suppression of the NLO correction relies on the fact that the perturbations $\beta, a_{\pm\mathbf{k}}$ introduced in section 2.3 have their “natural” order of magnitude ($a_{\pm\mathbf{k}} \sim \mathcal{O}(1), \beta \sim \mathcal{O}(gQ)$). If their equation of motion suffers from instabilities that amplify them, then the previous estimate is incorrect and the NLO corrections may be as large as the leading order contribution. It is therefore necessary to study the stability of small perturbations to the classical field φ .

To keep the discussion simple, let us assume in this appendix that the source J , and therefore also the classical field φ , do not have any spatial dependence²⁵. If $a(x^0, \mathbf{x})$ is a perturbation to the field φ , we can write its evolution equation in a linearized form as long as it remains small compared to the classical field φ itself,

$$\left(\square + \frac{g^2}{2}\varphi^2\right)a = 0. \quad (69)$$

This equation can be simplified by Fourier transforming the field $a(x^0, \mathbf{x})$ in the spatial variables²⁶,

$$a(x^0, \mathbf{x}) \equiv \int \frac{d^3\mathbf{k}}{(2\pi)^3} a(x^0, \mathbf{k}) e^{i\mathbf{k}\cdot\mathbf{x}}, \quad (70)$$

so that

$$\ddot{a} + (\mathbf{k}^2 + \frac{g^2}{2}\varphi^2)a = 0. \quad (71)$$

²⁵The results we obtain here remain valid in the case their spatial gradients are small.

²⁶We use the same symbol for a and for its Fourier transform to keep the notations light, as the context always allows one to distinguish the two.

(The dot denotes a derivative with respect to time.) Given a pair of solutions a_1 and a_2 of this equation, the Wronskian $W \equiv \dot{a}_1 a_2 - a_1 \dot{a}_2$ is independent of time.

When φ depends only on time, it is a periodic function of time at $x^0 > 0$. Therefore, the coefficient of the term $a(x^0, \mathbf{k})$ in eq. (71) is also periodic in time, which may lead to parametric resonance phenomena. For linear equations with periodic coefficients, the stability analysis can be performed by finding the “mapping at a period”, that evolves a pair of solutions $a_{1,2}$ from $x^0 = 0$ to $x^0 = T$ (where T is the period of the coefficients in the equation):

$$\begin{pmatrix} a_1(T, \mathbf{k}) & a_2(T, \mathbf{k}) \\ \dot{a}_1(T, \mathbf{k}) & \dot{a}_2(T, \mathbf{k}) \end{pmatrix} \equiv M_{\mathbf{k}} \begin{pmatrix} a_1(0, \mathbf{k}) & a_2(0, \mathbf{k}) \\ \dot{a}_1(0, \mathbf{k}) & \dot{a}_2(0, \mathbf{k}) \end{pmatrix}. \quad (72)$$

This mapping can be written as a multiplication by a matrix $M_{\mathbf{k}}$ thanks to the fact that equation (71) is linear. If the mapping $M_{\mathbf{k}}$ is known, then after n periods one has

$$\begin{pmatrix} a_1(nT, \mathbf{k}) & a_2(nT, \mathbf{k}) \\ \dot{a}_1(nT, \mathbf{k}) & \dot{a}_2(nT, \mathbf{k}) \end{pmatrix} \equiv M_{\mathbf{k}}^n \begin{pmatrix} a_1(0, \mathbf{k}) & a_2(0, \mathbf{k}) \\ \dot{a}_1(0, \mathbf{k}) & \dot{a}_2(0, \mathbf{k}) \end{pmatrix}, \quad (73)$$

and it is clear that the asymptotic behavior of the solutions $a_{1,2}$ is determined by the eigenvalues $\lambda_{1,2}$ of the matrix $M_{\mathbf{k}}$.

From the conservation of the Wronskian, it is immediate to get

$$\det(M_{\mathbf{k}}) = \lambda_1 \lambda_2 = 1. \quad (74)$$

The two eigenvalues are thus mutually inverse, and we can write the trace as:

$$\text{tr}(M_{\mathbf{k}}) = \lambda + \lambda^{-1}, \quad (75)$$

where λ is any of the two eigenvalues. One has therefore several cases:

- If $\text{tr}(M_{\mathbf{k}}) > 2$ (resp. $\text{tr}(M_{\mathbf{k}}) < -2$), then λ is real and greater than 1 (resp. smaller than -1). In this case, the solutions of eq. (71) generically diverge exponentially with time.
- If $\text{tr}(M_{\mathbf{k}}) = 2$ (resp. -2), then $\lambda = 1$ (resp. -1). The two eigenvalues of $M_{\mathbf{k}}$ are in fact equal to 1 (resp. -1). For $\lambda = 1$, this implies that the matrix $M_{\mathbf{k}}$ is of the form

$$M_{\mathbf{k}} = P^{-1} \begin{pmatrix} 1 & \alpha \\ 0 & 1 \end{pmatrix} P, \quad \text{and} \quad M_{\mathbf{k}}^n = P^{-1} \begin{pmatrix} 1 & n\alpha \\ 0 & 1 \end{pmatrix} P. \quad (76)$$

In this case, one of the solutions is T -periodic (and is therefore stable), while the other solution of the basis diverges linearly with time (unless $\alpha = 0$ accidentally).

- If $-2 < \text{tr}(M_{\mathbf{k}}) < 2$, the eigenvalues $\lambda_{1,2}$ are complex and lie on the unit circle, $\lambda_{1,2} \equiv \exp(\pm i\theta)$ (they are mutual complex conjugates since the matrix $M_{\mathbf{k}}$ is real valued). In this case, the small fluctuations are stable.

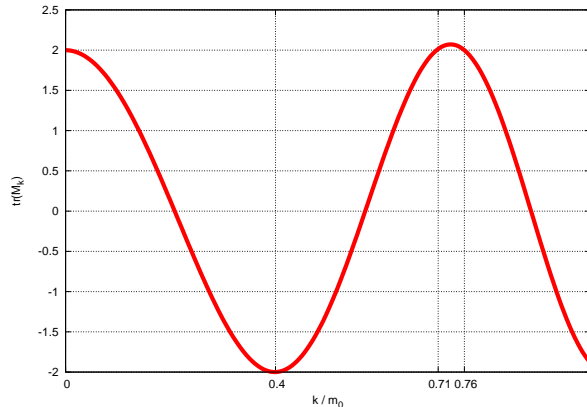


Figure 16: Trace of the monodromy matrix as a function of km_0 (we denote $m_0^2 \equiv \frac{1}{2}g^2\varphi_0^2$).

One can compute numerically the monodromy matrix $M_{\mathbf{k}}$ and its trace as a function of \mathbf{k} . We have displayed the result in the figure 16. We see that the trace is equal to 2 for a discrete set of modes, including the zero mode²⁷. There is a band of modes²⁸ $0.71 \leq k/m_0 \leq 0.76$ in which the trace is greater than 2, and where the fluctuations are exponentially unstable. Outside of these discrete modes and of the resonance band, the trace is between -2 and 2, and the fluctuations are stable. Besides these rigorous statements about the location of the unstable modes, in practice the modes \mathbf{k} for which $|\text{tr}(M_{\mathbf{k}})| < 2$ but is close to 2 display a linearly growing behavior for a rather long time, before they eventually decrease. For instance, modes near the zero mode grow linearly for a time of order $2\pi/k$ before they start decreasing. Strictly speaking, these modes are not unstable, but their growth at early times makes them important for the transient dynamics of the system.

B.2 Lyapunov exponent

In the resonance band, the exponential instability of the solutions of eq. (71) can be characterized by the Lyapunov exponent, that one can define from the largest eigenvalue of $M_{\mathbf{k}}$ as follows,

$$\mu(\mathbf{k}, m_0) \equiv \frac{1}{T} \ln \text{Max} \{ \lambda_{1,2} \}, \quad (77)$$

²⁷For $\mathbf{k} = 0$, it is easy to check that $a_1(t) \equiv \dot{\varphi}(t)$ and $a_2(t) \equiv \dot{\varphi}(t) \int_0^t d\tau / \dot{\varphi}^2(\tau)$ are solutions of eq. (71). Given these two solutions, it is straightforward to get $\text{tr}(M_0) = 2$.

²⁸In section B.2, we show that the boundaries of this band are in fact $1/\sqrt{2}$ and $1/3^{1/4}$.

where $m_0^2 \equiv \frac{1}{2}g^2\varphi_0^2$. Asymptotically, the solutions $a(x^0, \mathbf{k})$ of eq. (71) grow like

$$a(x^0, \mathbf{k}) \underset{x^0 \rightarrow +\infty}{\sim} e^{\mu(\mathbf{k}, m_0)x^0}. \quad (78)$$

The Lyapunov exponent can be obtained numerically from the trace of $M_{\mathbf{k}}$, but in the case of the ϕ^4 potential it can in fact be derived analytically²⁹. Consider the equation

$$\ddot{a} + (\mathbf{k}^2 + m^2(t))a = 0, \quad (79)$$

where

$$\ddot{m} + \frac{1}{3}m^3 = 0. \quad (80)$$

(In other words, $m(t) \equiv g\varphi(t)/\sqrt{2}$. The equation for $m(t)$ is a consequence of the equation for $\varphi(t)$.)³⁰ Let us call m_0 the maximal amplitude of the oscillations of $m(t)$, and introduce the new variable z defined by

$$m^2 = m_0^2 z. \quad (82)$$

The time t and the variable z are related by

$$\frac{dz}{dt} = m_0 \sqrt{\frac{2}{3}z(1-z^2)}, \quad (83)$$

and we can rewrite eq. (79) as

$$2z(1-z^2)a'' + (1-3z^2)a' + 3(\kappa^2 + z)a = 0, \quad (84)$$

where the prime denotes a derivative with respect to z and $\kappa \equiv k/m_0$. By this transformation, we have turned an equation with oscillating coefficients into an equation with polynomial coefficients. Given a pair $a_{1,2}$ of solutions of eq. (84), one can show that the Wronskian is

$$W \equiv a'_1 a_2 - a_1 a'_2 = \frac{w_0}{\sqrt{z(1-z^2)}}, \quad (85)$$

where w_0 is a constant.

Let us call now $M \equiv a_1 a_2$, with $a_{1,2}$ two solutions of eq. (84) (possibly identical). A straightforward calculation shows that M obeys the following third order differential equation:

$$2z(1-z^2)M''' + 3(1-3z^2)M'' + 6(z+2\kappa^2)M' + 6M = 0. \quad (86)$$

²⁹The derivation we expose here is a particular case of techniques developed in [30].

³⁰The value of g is not important per se. Only the combination $m_0 \sim g\varphi_0$ matters for the Lyapunov exponent. Moreover, if $\mu(\mathbf{k}, m_0)$ is the Lyapunov exponent, then it scales as

$$\forall \lambda, \quad \mu(\lambda\mathbf{k}, \lambda m_0) = \lambda \mu(\mathbf{k}, m_0), \quad (81)$$

due to the scale invariance of our model.

If a_1 and a_2 are two independent solutions of eq. (84), then the three independent solutions of eq. (86) can be thought of as a_1^2 , a_2^2 and a_1a_2 . A remarkable property of eq. (86) is that it admits a polynomial solution:

$$M(z) = z^2 - 2\kappa^2 z + 4\kappa^4 - 1. \quad (87)$$

If κ is in the resonance band, where a_1 increases exponentially while a_2 decreases exponentially, this polynomial solution must be their product $M(z) = a_1(z)a_2(z)$. With the help of the Wronskian, it is then easy to find

$$\begin{aligned} a_1(z) &= \sqrt{|M(z)|} \exp \left[+\frac{w_0}{2} \int^z \frac{dz}{M(z)\sqrt{z(1-z^2)}} \right] \\ a_2(z) &= \sqrt{|M(z)|} \exp \left[-\frac{w_0}{2} \int^z \frac{dz}{M(z)\sqrt{z(1-z^2)}} \right]. \end{aligned} \quad (88)$$

In order to determine the constant w_0 , one must insert these solutions into eq. (84). This leads to

$$w_0 = 4\sqrt{6\kappa^2 \left(\frac{1}{3} - \kappa^4\right) \left(\kappa^4 - \frac{1}{4}\right)}. \quad (89)$$

The resonance band corresponds to the values of κ such that the argument of the square root is positive (otherwise w_0 would be imaginary and one would have an oscillating solution instead of an exponentially growing solution). Thus, the instability domain is

$$\frac{1}{\sqrt{2}} \leq \kappa \leq \frac{1}{3^{1/4}}. \quad (90)$$

From the above solutions a_1, a_2 , one can also determine their growth during one period of oscillation of $m(t)$, from which one gets the Lyapunov exponent. One obtains

$$\mu(\mathbf{k}, m_0)T = 2w_0 \int_0^1 \frac{dz}{M(z)\sqrt{z(1-z^2)}}, \quad (91)$$

where T is the period of the oscillations of $m(t)$:

$$T = \frac{4\sqrt{6}}{m_0} \int_0^1 \frac{dz}{\sqrt{1-z^4}}. \quad (92)$$

We finally get:

$$\mu(\mathbf{k}, m_0) = 2m_0 \sqrt{\kappa^2 \left(\frac{1}{3} - \kappa^4\right) \left(\kappa^4 - \frac{1}{4}\right)} \frac{\int_0^1 \frac{dz}{(z^2 - 2\kappa^2 z + 4\kappa^4 - 1)\sqrt{z(1-z^2)}}}{\int_0^1 \frac{dz}{\sqrt{1-z^4}}}. \quad (93)$$

The integrals in this formula can be evaluated numerically³¹, and one can compare this analytical result to the direct numerical computation (performed by computing the trace of $M_{\mathbf{k}}$). As illustrated in the figure 17, the agreement is perfect.

³¹The integral in the numerator must be handled as a Cauchy principal value, since its integrand has two poles in the interval $z \in [0, 1]$.

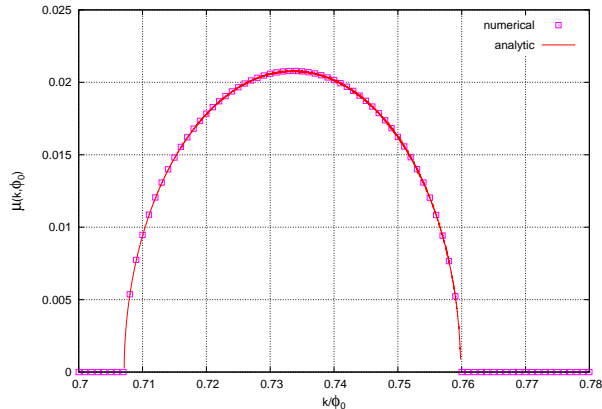


Figure 17: Comparison between a numerical computation of the Lyapunov exponent, and its evaluation from eq. (93).

B.3 Linear instability and time decoherence

Note that a zero Lyapunov exponent does not mean that the solutions are stable, it only implies that they are not exponentially unstable: outside of the resonance band determined by the inequality (90), the solutions of eq. (71) may exhibit a linear growth in time – either indefinitely if $\text{tr}(M_{\mathbf{k}}) = 2$ or during a finite time for all the other modes. In the case of the zero mode, this linear behavior has a very simple interpretation, because it is a direct consequence of the fact that the ϕ^4 potential leads to non-harmonic oscillations. Indeed, the classical field φ oscillates periodically in the potential with a frequency ω that is proportional to the amplitude φ_0 of the oscillations³²: a classical field that oscillates freely in a ϕ^4 potential can be written as

$$\varphi(t) = \varphi_0 f(\varphi_0 t), \quad (94)$$

where f is a periodic function of amplitude unity. Let us now add a small perturbation a to this classical field, so that its amplitude is now $\varphi_0 + a_0$. The perturbed oscillations are given by:

$$\psi(t) = (\varphi_0 + a_0) f((\varphi_0 + a_0)t). \quad (95)$$

If we assume that $a_0 \ll \varphi_0$ and we linearize in the perturbation, we have

$$\psi(t) = \varphi(t) + a_0 f(\varphi_0 t) + \varphi_0 a_0 t f'(\varphi_0 t) + \mathcal{O}(a_0^2). \quad (96)$$

³²This result is specific to a potential that has only a ϕ^4 term. Indeed, in four dimensions, such a field theory is scale invariant at the classical level, and its only dimensionful parameter is the amplitude of the oscillations of φ (set by the external source J that drives the system at $x^0 < 0$). For other potentials, the oscillation frequency ω is in general some complicated function of the amplitude φ_0 and of the coupling constants present in the potential.

The fact that the frequency depends on the amplitude produced a term that grows linearly with time for the linearized perturbation. This result is ubiquitous for any non-harmonic potential, and not specific to ϕ^4 . This is the reason why a linear instability is the generic behavior of the solutions of eq. (71). Due to its origin, this linear instability is also closely related to another property: two classical solutions that at $x^0 = 0$ differ only by a small perturbation a_0 will eventually become completely incoherent since their phase has shifted by 2π after a time of order

$$t_{\text{decoherence}} \sim \frac{2\pi}{a_0}. \quad (97)$$

In the case of perturbations that have a non-zero momentum \mathbf{k} , the scaling law (94) is not valid if $g\varphi_0 \lesssim |\mathbf{k}|$. For these high \mathbf{k} modes, the oscillations are almost harmonic and thus independent of their amplitude. This means that the linear growth becomes weaker and weaker as $|\mathbf{k}|$ increases, and practically irrelevant for Fourier modes above $g\varphi_0$.

References

- [1] J. Adams, et al., [STAR Collaboration] Nucl. Phys. **A 757**, 102 (2005).
- [2] K. Adcox, et al., [PHENIX Collaboration] Nucl. Phys. **A 757**, 184 (2005).
- [3] I. Arsene, et al., [BRAHMS collaboration] Nucl. Phys. **A 757**, 1 (2005).
- [4] B.B. Back, et al., [PHOBOS collaboration] Nucl. Phys. **A 757**, 28 (2005).
- [5] P. Romatschke, Int. J. Mod. Phys. E **19**, 1 (2010).
- [6] D. Teaney, Prog. Part. Nucl. Phys. **62**, 451 (2009).
- [7] G. Policastro, D.T. Son, A.O. Starinets, Phys. Rev. Lett. **87**, 081601 (2001).
- [8] G. Policastro, D.T. Son, A.O. Starinets, JHEP **0209**, 043 (2002).
- [9] T. Hirano, U.W. Heinz, D. Kharzeev, R. Lacey, Y. Nara, Phys. Lett. **B 636**, 299 (2006).
- [10] T. Lappi, R. Venugopalan, Phys. Rev. **C 74**, 054905 (2006).
- [11] H.J. Drescher, A. Dumitru, A. Hayashigaki, Y. Nara, Phys. Rev. **C 74**, 044905 (2006).
- [12] H. Song, U.W. Heinz, Nucl. Phys. **A 830**, 467C (2009).
- [13] M. Luzum, P. Romatschke, Phys. Rev. **C 78**, 034915 (2008), Erratum-
ibid.C **79**, 039903 (2009).
- [14] K. Dusling, G.D. Moore, D. Teaney, Phys. Rev. **C 81**, 034907 (2010).

- [15] P. Arnold, J. Lenaghan, G.D. Moore, L.G. Yaffe, Phys. Rev. Lett. **94**, 072302 (2005).
- [16] E. Iancu, R. Venugopalan, Quark Gluon Plasma 3, Eds. R.C. Hwa and X.N. Wang, World Scientific, hep-ph/0303204.
- [17] E. Iancu, A. Leonidov, L.D. McLerran, Lectures given at Cargese Summer School on QCD Perspectives on Hot and Dense Matter, Cargese, France, 6-18 Aug 2001, hep-ph/0202270.
- [18] F. Gelis, E. Iancu, J. Jalilian-Marian, R. Venugopalan, arXiv:1002.0333.
- [19] L.V. Gribov, E.M. Levin, M.G. Ryskin, Phys. Rept. **100**, 1 (1983).
- [20] A.H. Mueller, J-W. Qiu, Nucl. Phys. **B 268**, 427 (1986).
- [21] L.D. McLerran, R. Venugopalan, Phys. Rev. **D 49**, 2233 (1994).
- [22] L.D. McLerran, R. Venugopalan, Phys. Rev. **D 49**, 3352 (1994).
- [23] L.D. McLerran, R. Venugopalan, Phys. Rev. **D 50**, 2225 (1994).
- [24] T. Lappi, L.D. McLerran, Nucl. Phys. **A 772**, 200 (2006).
- [25] F. Gelis, T. Lappi, R. Venugopalan, Phys. Rev. **D 78**, 054019 (2008).
- [26] F. Gelis, T. Lappi, R. Venugopalan, Phys. Rev. **D 78**, 054020 (2008).
- [27] F. Gelis, T. Lappi, R. Venugopalan, Phys. Rev. **D 79**, 094017 (2009).
- [28] N. Goldenfeld, *Lectures on Phase Transitions and the Renormalization Group*, Frontiers in Physics, Addison Wesley (1992).
- [29] R. Allahverdi, R. Brandenberger, F. Cyr-Racine, A. Mazumdar, arXiv:1001.2600.
- [30] P.B. Greene, L. Kofman, A.D. Linde, A.A. Starobinsky, Phys. Rev. **D 56**, 6175 (1997).
- [31] R. Micha, I.I. Tkachev, Phys. Rev. **D 70**, 043538 (2004).
- [32] D.T. Son, hep-ph/9601377.
- [33] D. Polarski, A.A. Starobinsky, Class. Quant. Grav. **13**, 377 (1996).
- [34] S.Yu. Khlebnikov, I.I. Tkachev, Phys. Rev. Lett. **77**, 219 (1996).
- [35] T. Prokopec, T.G. Roos, Phys. Rev. **D 55**, 3768 (1997).
- [36] A.V. Frolov, JCAP **0811**, 009 (2008).
- [37] G.N. Felder, I.I. Tkatchev, Comput. Phys. Commun. **178** (2008).
- [38] J.M. Deutsch, Phys. Rev. **A 43**, 2046 (1991).

- [39] M. Srednicki, Phys. Rev. E **50**, 888 (1994).
- [40] C. Jarzynski, Phys. Rev. E **56**, 2254 (1997).
- [41] M. Rigol, V. Dunjko, M. Olshanii, Nature **452**, 854 (2008).
- [42] M.V. Berry, J. Phys. A: Math. Gen. **1012**, 2083 (1977).
- [43] T.S. Biro, C. Gong, B. Muller, A. Trayanov, Int. J. Mod. Phys. **C 5**, 113 (1994).
- [44] U.W. Heinz, C.R. Hu, S. Leupold, S.G. Matinyan, B. Muller, Phys. Rev. **D 55**, 2464 (1997).
- [45] T. Kunihiro, B. Muller, A. Ohnishi, A. Schafer, T.T. Takahashi, A Yamamoto, arXiv:1008.1156.
- [46] F. Gelis, R. Venugopalan, Nucl. Phys. **A 776**, 135 (2006).
- [47] F. Gelis, R. Venugopalan, Nucl. Phys. **A 779**, 177 (2006).
- [48] D. Boyanovsky, H.J. de Vega, R. Holman, D.S. Lee, A. Singh, Phys. Rev. **D 51**, 4419 (1995).
- [49] C.G. Callan, S.R. Coleman, R. Jackiw, Ann. Phys. **59**, 42 (1970).
- [50] F. Gelis, T. Lappi, R. Venugopalan, Int. J. Mod. Phys. E **16**, 2595 (2007).
- [51] K. Fukushima, F. Gelis, L. McLerran, Nucl. Phys. **A 786**, 107 (2007).
- [52] K. Dusling, F. Gelis, S. Srednyak, R. Venugopalan, work in progress.